A MUSCULOSKELETAL MODEL OF A SUBJECT SPECIFIC KNEE JOINT WITH MENISCI DURING THE STANCE PHASE OF A WALK CYCLE

A DISSERTATION IN
ENGINEERING AND MATHEMATICS

Presented to the Faculty of the University
of Missouri-Kansas City in partial fulfillment of
the requirements for the degree of
DOCTOR OF PHILOSOPHY

by
MOHAMMAD KIA

University of Missouri-Kansas City
2011

Copyright © by Mohammad Kia
2011

A MUSCULOSKELETAL MODEL OF A SUBJECT SPECIFIC KNEE JOINT WITH MENISCI DURING THE STANCE PHASE OF A WALK CYCLE

Mohammad Kia, Candidate for the Doctor of Philosophy Degree

University of Missouri – Kansas City, 2011

ABSTRACT

Movement simulation and musculoskeletal modeling can predict muscle forces, but current methods are hindered by simplified representations of joint structures. Simulations that incorporate muscle forces, an anatomical representation of the natural knee, and contact mechanics would be a powerful tool in orthopedics.

This study developed a subject specific computational model of the knee with menisci within the multibody framework. The model was validated with experimental measurements from a mechanical knee simulator and then it was incorporated into a neuromusculoskeletal model of a lower limb. The detailed model of a subject specific knee was developed in MD.ADAMS (MSC Software Corporation, Santa Ana, CA). This model includes femur, tibia, patella as well as lateral and medial meniscus geometries and knee ligaments of a subject specific cadaver knee (female: 78 years old, 59 kg right knee). A deformable contact with constant coefficients was applied to define the contact force between patella, femur, and tibia articular cartilages.

Meniscus geometries were divided into 61 discrete elements (29 medial and 32 lateral) that were connected through 6×6 stiffness matrices. An optimization and design of experiments approach was used to determine parameters for the 6×6 stiffness matrices such that the force–displacement relationship of the meniscus matched that of a linearly elastic transversely isotropic finite element model for the same cadaver meniscus. Similarly, parameters for compliant contact models of tibio-menisco-femoral articulations were derived from finite element solutions. As a validation step, the multibody knee model was placed within a dynamic knee simulator model and the tibio-femoral and patello-femoral kinematics were compared to an identically loaded cadaver knee.

Consequently, the validated knee model was incorporated into a scaled lower right limb musculoskeletal model in LifeMOD^{TM} (Lifemodeler, Inc.). A forward-dynamics muscle driven simulation of the stance phase of a gait cycle was simulated to estimate muscles and ground reaction forces. The predicted forces were evaluated using test data provided by Vaughan CL. et al. (1999).

The faculty listed below, appointed by the Dean of the School of Computer and Engineering have examined a dissertation titled "A Musculoskeletal Model of a Subject Specific Knee Joint with Menisci, During the Stance Phase of a Walk Cycle" presented by Mohammad Kia, candidate for the Doctor of Philosophy degree, and certify that in their opinion it is worthy of acceptance.

Supervisory Committee

Trent M. Guess, Ph.D., Committee Chair
Department of Civil and Mechanical Engineering

Ganesh Thiagarajan, Ph. D.
Department of Civil and Mechanical Engineering

Gregory W. King, Ph. D.
Department of Civil and Mechanical Engineering

Reza Derakhshani, Ph.D.
Department of Electrical and Computer Engineering

Hristo Voulov, Ph.D.
Department of Mathematics and Statistics

TABLE OF CONTENTS

TABLES

ILLUSTRATIONS

ACKNOWLEDGEMENTS

There is a phrase in Farsi, "*yek donya mamnoon.*" It means "a world of thanks." Sometimes I think "one world" may not be large enough to thank all the people who have supported me in accomplishing my educational goals.

I would like to start off by thanking Dr. Trent Guess, my advisor, for having faith in my abilities from the very beginning. His tremendous support has guided me through my doctoral studies. I would also like to express my gratitude to my committee, Dr. Ganesh Thiagarajan, Dr. Greg King, Dr. Reza Derakhshanee, and Dr. Hristo Voulov for their assistance, and support, along the way. I also want to thank all my fellow lab mates: Dr. Hongzeng Liu, Dr. Antonis Stylianou, Katherine Bloemker, Gavin Paiva, Leo Olcott, Paul Wilson, and Meenakshi Mishra, for their inspiration, support, and all the useful information they provided to me. Without them, I could not have finished my work studies.

Next, I would like to give my special thanks to my family in Iran which include: my parents, my sister, and my brother, for their love and spiritual support during this journey. I am also personally indebted to my extended family, in the U.S., who has offered me love, warmth, and hospitality throughout my life experiences in Kansas. Their presence made it feel like "home."

Finally, I have to give a huge THANKS to Michael Dix, my English tutor, for helping me understand some of the mysteries of the English language.

CHAPTER 1

INTRODUCTION

The absence of detailed knowledge regarding mechanical loading on knee soft tissues, particularly the menisci, inhibits our understanding of menisci degenerations and injuries. Different computational modeling techniques have been used to understand and enhance this knowledge. In recent years, several finite element models of the knee joint that include menisci have been developed [Donahue TL. et al. 2002, Zielinska B. and Donahue TL. 2006, Yang NH. et al. 2010]. The advantage of finite element models consists of their ability to evaluate and predict the stress and strain on soft tissue in articulating contacts. However, finite element models are computationally expensive and they are difficult to be used in concurrent dynamic simulations. Generally, static forces or tibio-femoral kinematics are used as inputs in these models and representations of individual muscles are ignored. In contrast to the finite element models, multibody dynamic musculoskeletal models are computationally efficient and can be used in concurrent simulations to predict muscle forces during complex activities. The major weaknesses of multibody musculoskeletal models are idealizations of the joints as well as simplifications of knee geometries.

The aim of this work was to develop a multibody musculoskeletal model that simultaneously predicts muscle forces and tibio-menisco-femoral contact. This knowledge

would provide valuable insight to the *in vivo* loading environment of knee tissue during motions. In order to improve soft tissue modeling techniques, a 3-D computational knee model with representation of the menisci in a multibody frame-work was developed. This model includes the femur, the tibia, and the patella as well as the lateral and medial meniscus geometries and knee ligaments of a subject specific cadaver knee (female: 78 years old, 59 kg right knee). The first hypothesis to be tested in this study was that removing the menisci will inevitably increase the total contact forces across the knee joint. Secondly, we examined the hypothesis that the menisci act as a stabilizer within the knee joint and effect knee kinematics.

1.1 Introduction to the Menisci Anatomy

The knee structure can be traced back to more than 300 million years, to the pelvic appendages of Sarcoptorigian lobe-finned fish [Dye SF. 2003]. In order to better understand menisci functions, it is important to review some basic anatomy, and biomechanical properties of the menisci. Furthermore, knowledge of menisci ligaments is necessary in order to correlate meniscus anatomy to meniscus function.

The menisci of the knee act primarily to transmit and redistribute contact force over the tibia plateau. This function of the menisci is achieved through a combination of material, geometry, and attachments. The menisci are two semicircular fibrocartilage structures that are found within the knee joint between the femur condyles and tibia plateau. For many years the menisci were considered as functionless structures. Indeed in 1887, Sutton JB stated that menisci are functionless remains of a leg muscle. Over the past century attitudes toward menisci and menisical surgery have changed.

Numerous studies have shown that the menisci play important roles in load distribution [Donahue TL. et al. 2002, Andriacchi TP. et al. 2004, Yang NH. et al. 2010], load bearing [Bullough PG. et al. 1997, Fukubayashi T. et al. 1980, Seedhom BB. 1976] shock absorption [Kurosawa H. et al. 1980, Krause WR. et al. 1976], and joint stability [Fukubayashi T. et al. 1982, Levy IM. et al. 1982 and 1989, Markolf KL. et al. 1981]. It also has been proven that they have sensory function, proprioception [Messner K. and Gao J. 1998] as well as lubrication roles within the knee joint [Renstorm P. and Johnson RJ. 1990].

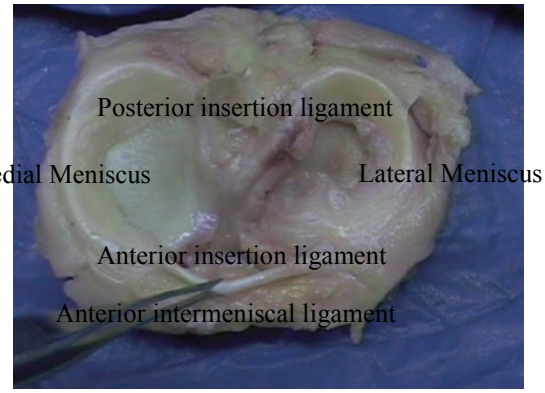

Figure 1.1 : Menisci anatomy and associated structures [Beaufils P. 2010]

The menisci (medial and lateral meniscus) are wedged shaped in cross section and they cover approximately two thirds of the corresponding tibio-femoral joint surface [Englund M. et al. 2008]. Each meniscus is attached to the tibia plateau anteriorly and posteriorly via insertion ligaments or horn attachments (Fig. 1.1). Menisci attachments are critical for proper menisci functions. It has been shown that, in rabbits, transection of the anterior or posterior insertion ligaments of the menisci would lead to osteoarthritis (OA) after 6 to 12 weeks [Sommerlath K. and Gillquist J. 1992]. Similarly, the meniscal release procedure, which consists of transection of the medial meniscus horn attachments, produces joint degeneration and osteoarthritis in the canine stifle (knee) joint [Stylianou. A, et al.

2011]. The medial and lateral menisci are connected to each other with the anterior intermeniscal ligament also known as the anterior transverse ligament. The functional role of this ligament is to control the relative positioning of the menisci on the tibia plateau when the tibia rotates [Nelson EW. and LaPrade RF. 2000].

Both the medial and lateral menisci translate posteriorly on the tibia plateau as the knee flexes. The lateral meniscus is more mobile than the medial one [Yao J. et al. 2008]; this is because the lateral meniscus is not attached to the tibia as tight as the medial meniscus. In addition, the medial tibial plateau is concave whereas the lateral tibial plateau is convex, which allows the lateral meniscus to translate more posteriorly in deep flexion [Yao J. et al. 2008]. This asymmetric kinematics between the medial and lateral component results in an internal rotation of the tibia relative to the femur with increasing flexion angle [Beaufils P. and Verdonk R. 2010].

Several studies have investigated the tensional properties of the menisci [Fithian DC. et al. 1990, Goertzen DJ. et al. 1997, Lechner K. et al. 2000, Messner K. and Gao J. 1998]. All studies revealed that the menisci are stiffer in the circumferential direction because the Type I collagen fibers are oriented primary in the circumferential direction of each meniscus [Yang NH. et al. 2010]. Menisci tensile strength varied from 80 - 125 MPa in the circumferential direction and only 1.7-3.6 MPa in the radial direction [Tissakht M. and Ahmed AM. 1995]. Also the menisci appear to be significantly stiffer in tension than compression (approximately 0.15MPa compression strength) [Joshi MD. et al. 1995, Proctor CS. et al. 1989, Sweigart MA. et al. 2004]. These characteristics render the menisci highly deformable allowing them to conform to the variable geometry of the femoral condyles during knee flexion-extension.

The menisci are often ignored in multibody computational models, due to their complexity and difficulty to model [Arnold EM. et al. 2009, Sasaki K. and Neptune RR. 2010]. Only a few studies have tried to address this issue. For example, Li G. et al. (2001-2002) used nonlinear spring elements to simulate the equivalent resistant of menisci. Pena E, et al. (2005) used finite element method to model the meniscus to study effect of meniscectomies and menisci tear on human knee biomechanics. In his study the meniscus was modeled as a continuous material with isotropic properties [Pena E. et al. 2005, 2006a, 2006b 2008]. A few other studies have modeled the menisci as a transversely isotropic material [Donahue TL. et al. 2002, Zielinska, and Donahue TL. 2006, Yang NH. et al. 2010]. Although finite element models can provide important information regarding tissue interaction under static or quasi-static boundary conditions, they are very time consuming to simulate menisci behaviors in dynamic activities.

1.2 Introduction to the Musculoskeletal Modeling Techniques

Musculoskeletal modeling and movement simulation can estimate individual muscle forces and provide insight to motor control and joint loading. The inverse dynamics method can predict net joint forces and torques using measured ground reaction forces, motion, and anthropometrics. Optimization methods can then be used to predict the muscle forces that reproduce the net loads at a joint and that meet an optimization objective such as minimization of muscle force. The forward dynamics method calculates the muscle forces to reproduce predicted joint motions and torques, based on the resultant inverse dynamics solution. Typically, an optimization method that requires many iterative simulations to find

muscle activation patterns was applied, to minimize differences between experimental and predicted movement [Erdmeir A. et al. 2007].

Also electromyography (EMG) measurements can be used directly to drive a forward dynamic simulation and quantify muscle forces [Piaza SJ. and Delp SL. 2001]. However, most clinical studies use EMG to verify estimated muscle forces instead [Sasaki K. and Neptune RR. 2010]. Currently, neuromusculoskeletal modeling involves simplifications of the joints (e.g. the knee presented as a simple hinge joint) and models are developed within a multibody (rigid body dynamics) framework. Concurrent simulation of motor control and tissue response may be essential for understanding knee degeneration and injury. Although the finite element method is necessary for the determination of strain within tissue, dynamic multibody models that have the computational efficiency for musculoskeletal modeling that also incorporate interactions of joint organs. Such models can be a valuable tool in understanding joint functions in dynamic situations. A review of published quasi-static [Blankevoort L. et al. 1991, Pandy MG, et al. 1998] and dynamic [Garuntu DI. et al. 2004, Bei Y. et al. 2004] 3D multibody natural knee models reveals that none include representation of the menisci.

Dynamic multibody musculoskeletal models that simultaneously predict muscle forces and tibio-menisco-femoral contact would provide valuable insight to the *in vivo* loading environment of knee tissue during ambulatory activities. A better understanding of *in vivo* mechanical loads has implications for the development and progression of osteoarthritis. For example, 43% of patients with intact anterior cruciate ligaments and isolated limited meniscectomy had radiographic evidence of osteoarthritis after 16 years [Englund M. et al. 2003]. In addition, the severity of osteoarthritis correlated with the

severity of meniscal injury and the amount of tissue removed [Englund M. et al. 2004]. It is generally believed that a significant contributor to cartilage degeneration after meniscectomy is the change in mechanical loading. Tissue engineering of the knee meniscus [Guilak F. et al. 2001], meniscus allograft replacement surgery [Sohn DH. and Toth AP. 2008], and development of artificial menisci replacements [Van T. et al. 2009] would all benefit from models that predict tibio-menisco-femoral biomechanical interactions during everyday activity.

Presented here is a method to develop a musculoskeletal model of a human knee joint that includes the menisci. The aims of this study are to demonstrate the interaction between the muscles, soft tissues, knee contact mechanics, and ground reaction forces during the stance phase of a walk cycle. The geometry of the distal femur, proximal tibia, patella, medial and lateral meniscus is provided based on a cadaveric knee. The compliant deformable contacts are applied in articulation surfaces of the femur, tibia, patella, and menisci. The meniscus model includes discrete elements connected through 6×6 stiffness matrices. Parameters of the 6×6 spring coefficient matrices are optimized such that the force–displacement relationship of the meniscus matched that of a finite-element solution for the same cadaver knee. Similarly, parameters for compliant contact models are derived from a finite element model solution. Twenty five spring-damper elements describe the mechanical properties of the collateral ligaments, cruciate ligaments, patella tendons, and menisci horn attachments. In order to validate the mechanical behaviors of the knee model, it is placed within a previously validated dynamic knee simulator model [Stricklan AM. 2009] and the tibio-femoral and patello-femoral kinematics are compared to the identically loaded cadaver knee (Fig. 1.2).

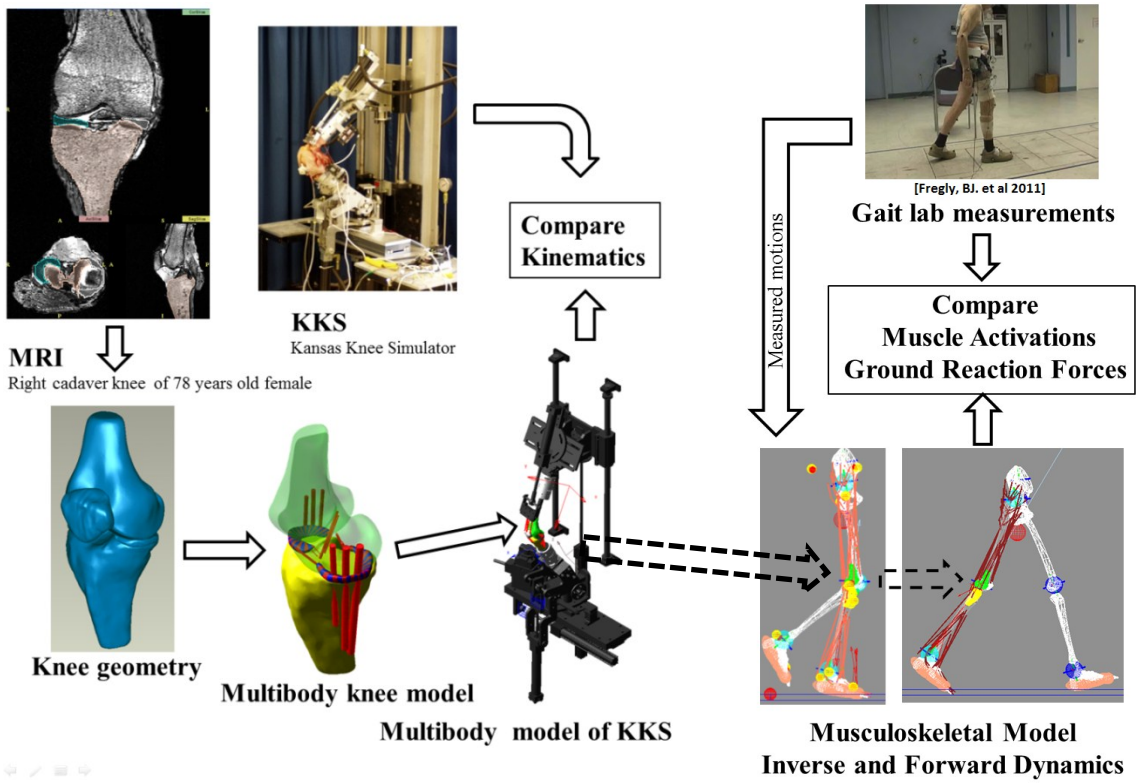

Figure 1.2: Schematic with overall view of the entire project

. In the final step, the validated knee model is incorporated into a scaled lower right limb musculoskeletal model in LifeMOD^{TM} (Lifemodeler, Inc.). Forty-five "trainable" muscle units are included in this model to record the muscle contraction while an inverse dynamics simulation is performed. The trained muscle elements are modeled as proportional–integral–derivative controllers. In order to perform the inverse dynamics simulation the musculoskeletal model is actuated with measured motion data to simulate the stance phase of a walk cycle (from the initial double support stance to the single support). Then, a forward-dynamics muscle driven simulation of the stance phase profile is simulated to estimate muscle forces (Fig. 1.2). The predicted forces are evaluated using the test data provided by Vaughan CL. et al. (1999).

CHAPTER 2

MATERIALS AND METHODS

2.1 Cadaver Knee Measurements and Testing

A 78-year-old female right cadaver knee was used for this study. The specimen weight at death was 130 lb (59 kg) and the knee was frozen until the day of testing. The knee appeared normal and intact during visual inspection. Knee geometries were created from magnetic resonance images (Siemens 1.5 T machine with kneecoil). Three 512×512 resolution imaging sequences were obtained including two sagittal plane sequences (0.7mm slice thickness,TR:13.64, TE:6.82 and 1mm slice thickness, TR:45, TE:17) and a frontal plane sequence (1mm slice thickness, TR:13.64, TE:6.82).Manual segmentation was then used to create geometries of the articular cartilage, bone, menisci, and ligaments using 3D Slicer (www.slicer.org). Post-process filtering and file conversion of the geometries was performed in Geomagic Studio (Geomagic, Inc. Research Triangle Park, NC). After imaging, the cadaver knee was placed in a dynamic knee simulator (Kansas Knee Simulator, University of Kansas, Lawrence, KS). The knee simulator replicates the loading and motion of physiological activities, such as walking, using five axes controlled through servo-

hydraulic actuators (quadriceps force, vertical force applied at the hip, medial–lateral ankle force, ankle vertical torque, and ankle flexion force) [Maletsky LP. and Hillberry BM. 2005]. Both position and force were measured at each axis and loading profiles for the machine were generated from a previously validated computational model [Guess TM. and Maletsky LP. 2005]. Several laxity, squat, and walking profiles were tested on the specimen knee. During testing, rigid body markers were attached to the femur, tibia, and patella and kinematics of each were recorded using a 3-camera Optotrak 3020 system (Northern Digital Inc., Waterloo, Ontario). For a 10◦ rotation, this system has a measurement bias of 0.05◦ and a 95% repeatability limit of 0.67◦. A 10-mm translation showed a bias of 0.03mm and a 95% repeatability limit of 0.29mm [Maletsky LP. et al. 2007]. The position and orientation of the cadaver femur and tibia relative to the knee simulator was determined by recording a series of 3D points (point clouds) along the articulating surfaces of the femur and tibia along with reference positions on the simulator. Point clouds were also collected at the anterior cruciate ligament (ACL), posterior cruciate ligament (PCL), medial collateral ligament (MCL), and lateral collateral ligament (LCL) origin and insertion sites. In addition, a quasi-static knee tester was used to obtain the laxity envelope-of-motion for each knee allowing for calculation of ligament bundle zero-load lengths (lengths at which particular ligament bundles first become taut).

2.2 Multibody Knee Model

2.2.1 Multibody Menisci Models

An anatomically based computational model of a right natural knee was created from subject specific medical images and experimental measurements of a cadaver knee. Geometries of the cadaver menisci were used to create multibody models in MD Adams

(MSC Software Corporation, Santa Ana, CA). A macro was written to divide the lateral and medial menisci geometries into 32 and 29 pieces respectively (Fig. 2.1). The macro calculated the geometric center of each meniscus and radially sectioned its geometry. The macro also assigned mass properties to each section based on its volume and a density of 1100 kg/m^3.

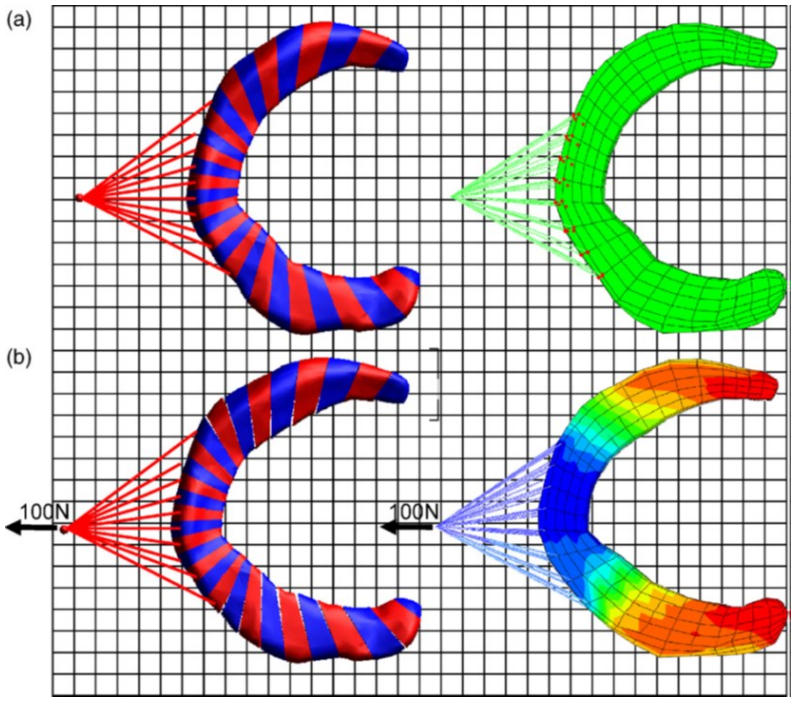

Figure 2.1 : Multibody and finite element models of the medial meniscus before (a) and after (b) a 100N load was applied in the medial direction

Meniscus geometries were then connected to neighboring geometries by the following stiffness matrix:

$$\begin{bmatrix} F\theta \\ Fr \\ Fz \\ T\theta \\ Tr \\ Tz \end{bmatrix} = \begin{bmatrix} K_\theta & K_{\theta r} & K_{\theta z} & 0 & 0 & 0 \\ K_{\theta r} & K_r & K_{rz} & 0 & 0 & 0 \\ K_{\theta z} & K_{rz} & K_z & 0 & 0 & 0 \\ 0 & 0 & 0 & T_\theta & 0 & 0 \\ 0 & 0 & 0 & 0 & T_r & 0 \\ 0 & 0 & 0 & 0 & 0 & T_z \end{bmatrix} \begin{bmatrix} \theta \\ r \\ z \\ a \\ b \\ c \end{bmatrix} \quad (2\text{-}1)$$

Where $F\theta, Fr, Fz$ and $T\theta, Tr, Tz$, are the translational forces and torsional moments between elements acting in the circumferential, radial, and axial directions.

$K_\theta, K_r, K_z, K_{\theta r}, K_{\theta z}, K_{rz}, T_\theta, T_r$ and Tz are the stiffness matrix parameters, θ, r, and z are translational displacements and a, b, and c are rotational displacements relative to the initial matrix locations. The same stiffness matrix parameters were used to connect each element of either the medial or lateral meniscus. Different stiffness parameters were defined for the lateral side and medial side. An optimization and design of experiments approach (DOE) that minimized the displacement error between identically loaded finite element and multibody menisci models was used to determine the stiffness matrix parameters for the medial and lateral menisci. The Finite Element models of menisci were defined using linearly elastic transversely isotropic materials with Young's modulus of 150MPa in the circumferential direction and 20MPa in the axial and radial directions [Donahue TL. et al. 2002]. Poisson's ratio was 0.2 in both circumferential and radial directions and it was 0.3 in the axial direction [Zielinska B. and Donahue TL. 2006]. The density of the meniscus was 1100 kg/m^3 [Fithian D. et al. 1990].

The DOE or design of experiment method is a statistical and mathematical tool to identify, optimize, and analyze the results of an experiment or simulation. In this study, DOE was applied to compare and obtain the optimal fit between the Multibody model and the predicted Finite Element force–displacement response.

Identical boundary conditions were defined for finite element and multibody models such that elements at the horn attachment sites of each meniscus were fixed and a single force was applied along the periphery of the tissue (Fig. 2.1). The force amplitude linearly increased from 0 to 100N in 1 sec. A medial load was applied to the medial meniscus and a

lateral load applied to the lateral meniscus. Displacement along the axis of force was measured as a function of time. The root mean square (RMS) displacement error between finite element and multibody model during the 1 sec loading time was defined as an objective function. A two-level fractional factorial design including nine variables was used as a screening algorithm. A tolerance level of 50% was assumed for each factor in this step and 64 simulations were run. After the initial screening step, new initial values were selected and a two-level fractional factorial design was used to determine which factors were statistically significant on meniscus displacement. For this step, the tolerance area was 10% for each factor. The confidence of the results was confirmed by checking the adjusted coefficient of determination (Radj> 0.9, and P < 0.005). As a final step, a higher order experimental plan (cubic model) was implemented to find the best possible values based on a non-linear model of significant factors.

2.2.2 Multibody Tibio-Femoral Model

A tibio-femoral joint model was created in MD Adams using the tibia, femur, and cartilage geometries. A compliant contact force model was used to provide a computationally efficient characterization of tibio-femoral cartilage contact. The contact model used in this study is a common representation based on Hertzian contact model with the addition of a damper to allow for energy dissipation [Sharf I. and Zhang Y. 2006]. Contact force as a function of local penetration was defined as:

$$F = k_c \delta^{exp_c} + B_c(\delta)\dot{\delta} \qquad (2\text{-}2)$$

Where k_c, exp_c, and B_c are parameters defining the contact between tibio-femoral articulating cartilage. A barrier to accurate contact simulation is the difficulty in determining contact parameters for complex materials and contact scenarios [Sharf I. and Zhang Y. 2006]. In this study, the contact model parameters were defined as design variables that were systematically modified during an optimization process to match a solution set from the identical finite element model of the knee joint.

The finite element model is discussed in detailed in a master's thesis by Mishra M. (2010). The following is a short description of the finite element model. This model includes femur, tibia, anterior cruciate ligament (ACL), medial collateral ligament (MCL) and articular cartilage geometry. The finite element model was developed and evaluated based on a study provided by Donahue TL. (2002). In this model the tibia was model as a rigid body and the femur was considered as a deformable body. The femur and tibia were meshed with their articulating cartilage geometry. The femur bone was defined as an isotropic material with a Young's modulus of 20 GPa, a Poisson's ratio of 0.2, and a density of 1600 kg/m^3 [Zielinska B. and Donahue TL. 2006]. The distal elements of the femur and proximal elements of the tibia were identified as cartilage, giving a cartilage thickness of approximately 4mm. The cartilage was specified as an isotropic material with Young's modulus of 15 MPa, Poisson's ratio of 0.475, and density of 1000 kg/m^3 [Zielinska B. and Donahue TL. 2006]. The ligaments were represented by one-dimensional linear spring elements that connected the femur and tibia. The ACL and MCL stiffness were assumed to be 3200 and 1600 N/mm [Donahue TL. et al. 2002].

During simulation, the tibia in both the finite element and multibody models were constrained from rotating in flexion– extension. In addition, the proximal femur was fixed.

A compressive axial load that linearly increased from 0 to 800N in 1 sec was then applied to the distal tibia, same as Donahue TL. et al. (2002) study. The displacement at the load application point was measured and the compliant contact parameters of Eq. (2-2) were optimized to minimize the three axes of translational displacement error between the two models. The method used to determine the cartilage–cartilage contact parameters was similar to that used to determine the menisci stiffness matrix coefficients. A two-level full factorial design was used for initial screening. After screening, a two-level (k_c and exp_c) full factorial design was used and finally a higher order cubic model (32 simulations) was used to find the contact parameters that best fit finite element model solutions.

2.2.3 Multibody Tibio-Menisco-Femoral Model

In order to determine parameters for the compliant contact between menisci and tibio-femoral cartilages, the menisci were added to the knee model. The meniscus macro was modified to add a compliant contact between each meniscus element and the tibia and femur cartilage geometries. The compliant contact was defined by:

$$F = k_m \delta^{exp_m} + B_m(\delta)\dot{\delta} \tag{2-3}$$

Where δ is the interpenetration of geometries and k_m, exp_m, and B_m are parameters defining the contact between the meniscus and cartilage. $\dot{\delta}$ is defined as a derivative of the interpenetration.

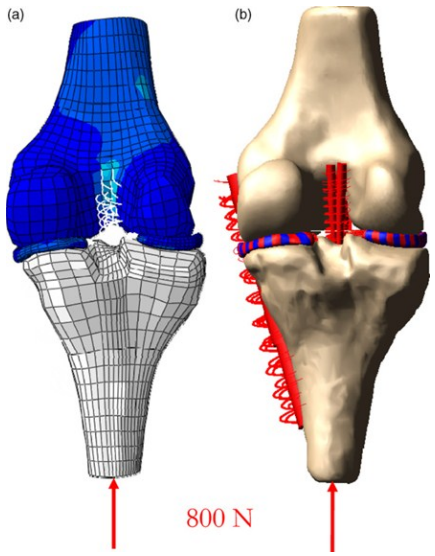

Figure 2.2: Finite element (a) and multibody (b) models of the tibio-femoral joint with menisci

Compliant contacts were defined between the cartilage geometries using Eq. (2-2) and (2-3). Previously optimized contact parameters were used. Similar to determining the cartilage-cartilage contact parameters, this model was compared to an identical finite element model [Mishra M. 2010]. This model includes tibio-femoral cartilage contact as well as tibio-menisco-femoral contacts.

The menisci were connected to the tibia via multiple spring elements at the horn attachment sites. Locations of the horn insertions were determined by physically probing the cadaver knee and from MRI. The total spring constant for each horn attachment was 2000N/mm [Donahue TL. et al. 2002].

The same loading and boundary conditions used for tibio-femoral simulations were applied to both the finite element and multibody models (Fig. 2.2). The meniscus–cartilage compliant contact parameters of Eq. (2-3) were then optimized such that the displacement error along the inferior–superior axis between the finite element and multibody was minimized.

2.2.4 Multibody Knee Model

Next, the multibody model of knee with menisci was constructed within a multibody model of the dynamic knee simulator and resulting tibio-femoral and patello- femoral kinematics compared to experimental measurements. In addition, the total loading on tibio-femoral articular cartilage was predicted during the simulation. The position and orientation of the tibia and femur geometries relative to the knee simulator was determined by recording a series of points (point clouds) along the femur and tibia as well as reference position points on the dynamic knee simulator. Rigid body markers attached to the femur, tibia, and patella defined experimental coordinate systems. Point clouds of the articulating surfaces and ligament insertions were collected in their respective coordinate systems after testing and disarticulation of the knee. A least squares curve fit between the point clouds and bone geometries was used to transform geometries from the MRI coordinate system to the experimental coordinate system. After placing bone and cartilage geometries of the tibia, femur, and patella within the simulator model (Fig. 2.3), compliant contacts were defined between cartilage–cartilage articulating surfaces using Eq. (2-2) and the previously determined parameters. The menisci models were then placed into the model using the tibial coordinate transformation and compliant contacts of Eq. (2-3).

Ligament bundles were represented as one-dimensional nonlinear springs. The model included two bundles for the ACL and PCL and three bundles for the MCL and LCL. The origin and insertion sites were determined from MRI and from point clouds obtained by physically probing the cadaver knee. Non-linear splines were used to describe the force–displacement curve of each ligament including the non-linear “toe” region. The splines were derived from the ligament force as a function of strain, the length of each ligament in the

position it was constructed, and the measured zero-load length. The force–length for each ligament is described [Blankevoort L. et al. 1991, Wismans J. et al. 1980] by:

$$f = \begin{cases} \frac{1}{4} k\varepsilon^2/\varepsilon_1 & 0 \le \varepsilon \le 2\varepsilon_1 \\ k(\varepsilon - \varepsilon_1) & \varepsilon > 2\varepsilon_1 \\ 0 & \varepsilon < 0 \end{cases} \quad (2\text{-}4)$$

$$\varepsilon = \left(\frac{l - l_0}{l_0}\right) \quad (2\text{-}5)$$

Where k is a stiffness parameter and ε is defined as the engineering strain. The spring parameter ε_1 is a constant value and it is assumed to be 0.03 to include the non-linear "toe" region [Li G. et al. 1999]. Values of k for each ligament bundle came from Wismans J. et al. (1980) and Blankevoort L. et al. (1991), table 2.1. The zero-load lengths of each ligament bundle were derived from the laxity envelope-of-motion measured on the cadaver knee. The maximum straight line distance between insertion sites of each ligament bundle during the laxity test was mapped and then multiplied by 0.85 to obtain the zero-load lengths for the relative position of the femur and tibia. Each spring element also included a parallel damper and a damping coefficient of 0.5Ns/mm was used for each ligament bundle.

Table 2.1
Ligament stiffness and zero-load length parameters

Knee Ligament	Ligament bundle	Stiffness Parameter (N)	Zero-load length Experimental (mm)
ACL	Anterior	5000	31.2
	Posterior	5000	24
PCL	Anterior	9000	24.8
	Posterior	9000	30.4
LCL	Anterior	2000	47.2
	Central	2000	45.6
	Posterior	2000	48.8
MCL	Anterior	2750	72.8
	Central	2750	80.8
	Posterior	2750	82.4

The patellar tendon was divided into three bundles with origins and insertions determined from cadaver point clouds. The quadriceps tendons were represented with four bundles with insertions on the patella and origins on a quadriceps clamp attached to the quadriceps force actuator. Patellar and quadriceps tendon force–length relationships were based on Piazza. S. and Delp. S. (2001) study. The model also simulated wrapping of the patellar tendon around the tibia geometry. Each spring representing a patellar tendon bundle was divided into two springs in series. The springs were then connected by an anatomically sized ellipsoid and positioned to create contact on the appropriate bone surfaces. Ellipsoid shapes were determined from MRI tendon cross-sections. A deformable contact was then defined between each ellipsoid and the tibia bone geometry.

The menisci were attached to the tibial plateau via horn attachments. Two one-dimensional springs were used to represent each attachment. Each spring had a stiffness of 1000N/mm in tension and 0N/mm in compression [Donahue TL. et al. 2002], with the zero-load lengths determined by the unloaded MRI position. The transverse ligament was also included with insertions measured on the cadaver knee. The transverse ligament was a 1D spring with a stiffness of 200N/mm in tension and 0N/mm in compression [Donahue TL. et al. 2002]. A parallel damper with damping coefficient of 0.5Ns/mm was included for each horn attachment and the transverse ligament spring.

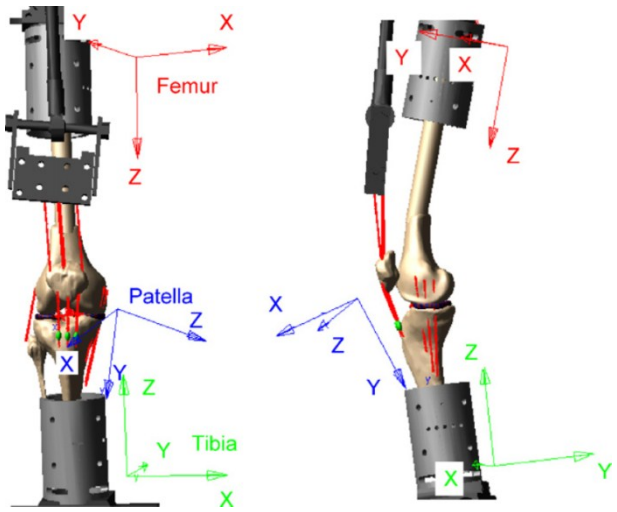

Figure 2.3. Picture of the knee model in the knee simulator. Also shown is the femur, tibia, and patella coordinate systems. The z-axis of the femur coordinate is approximately aligned with the long axis of the femur. The y-axis of the femur coordinate is primarily in the anterior–posterior direction while the x-axis is primarily oriented in the medial–lateral direction.

2.3 Multibody Knee Model Simulation

To verify the subject specific multibody knee model, a "modified" walking profile in the knee simulator was simulated on both the cadaver knee and virtual knee and the resulting bone kinematics compared. The walk cycle was based on ISO specification 14243-1(2002) and the actuators of the dynamic knee simulator were controlled to reproduce the loading and motion of this walk cycle at the knee. For one gait cycle, heel strike occurs at~0%of the cycle, mid-stance occurs at~20%, and toe-off occurs at ~60% of the cycle. Due to limitations of the dynamic knee simulator and to protect the cadaver knee, the walk cycle was modified such that the duration of each cycle was increased to 10 seconds. Measured hip flexion angle during experimental testing provided one of the model simulation inputs. A feedback control loop in the model adjusted the quadriceps force such that the desired hip flexion angle was maintained.

The dynamic knee simulator was controlled in a similar manner and the resulting quadriceps force from both model and experiment were compared. The other simulation inputs included the measured load from the remaining four servo-hydraulic actuators on the machine (vertical load at the hip, and three loads applied at the ankle). These loads were applied to force vectors in the model.

Measured kinematics included the position and orientation of the tibia and patella coordinate systems relative to the femur coordinate system (Fig. 2.3). Measurements included the x, y, and z translation of the tibia and patella origins relative to the femur origin represented in femoral coordinates and body 1, 2, and 3 orientation angles (1,2,3 Euler angle sequence) relative to the femur. The z-axis of the femur was aligned along the femoral shaft while the x- and y-axes were approximately aligned in the medial–lateral anterior–posterior directions of the femur.

2.4 Musculoskeletal Model

LifeMOD™ (LifeModeler, Inc., San Clemente, CA) was used to develop a generic musculoskeletal model of the human lower extremity. The generic model consisted of the lower torso, upper and lower leg segments and feet (Fig 2.4). Tri-axis hinges combined with passive torsional spring-damper torques were employed to model the hip, ankle and knee joints for both sides of the lower limb. Spring stiffness of 1e+4 N.mm/deg and damping coefficient of 1000 N.mm.s/deg was assumed for each simplified joint (Fig. 2.4). The knee joints were only allowed to rotate in flexion- extension direction.

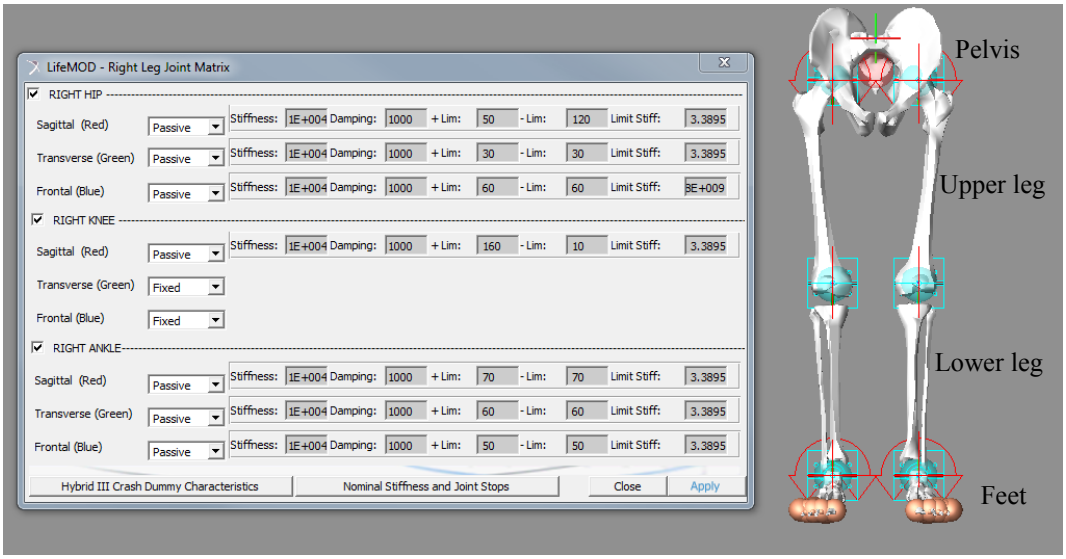

Figure 2.4: The generated model segments and joint base set properties

The gate data provided by Christopher L Vaughan et al. (1999) was used to scale and drive the model. Provided experimental set included motion data, ground reaction forces and surface electromyography during a stance phase of a gate cycle on a female subject with a calculated height of ~ 150 cm and total body mass of 51.2 kg; comparable to the cadaver knee (165 cm height and 59 kg weight). The subject's height was estimated based on the

anthropometric figure from Winter DA. (2009) that expressed body segments lengths as a fraction of body height (Fig. 2.5.).

Vaughan, in his experiment, applied a modified Helen Hays marker set to capture bilateral three dimensional motions using the VICON system. Marker locations were measured at a frequency of 50 HZ. Anthropometric measurements from the test subject were used to scale the generic model in LifeMod (Table 2.2). Then the developed multibody model of right knee was replaced with the right revolute joint in the generic model (Fig. 2.5). The knee joint was aligned such that the epicondylar axis was matched with the revolute joint mechanical axis. The femur and tibia of the knee were rigidly attached to the upper and lower leg segments of the generic model.

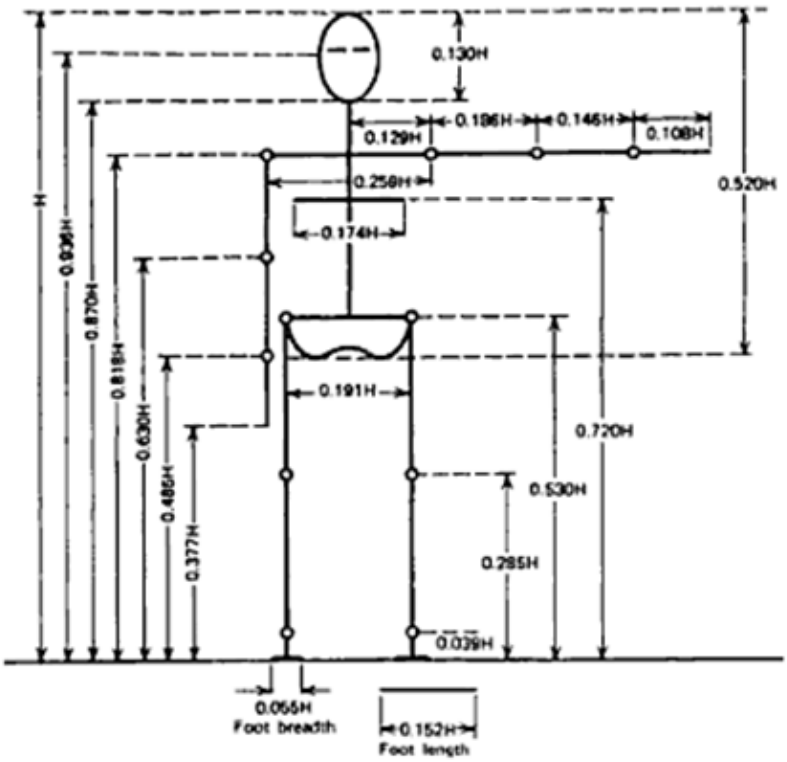

Figure 2.5: Segments' length expressed as a function of body height [Winter DA. 2009]

Table 2.2
Measured anthropometric data from a female subject [Vaughan CJ. et al. 1999]

Number	Anthropometric measurement	Value	Units
1	Total body mass	51.2	kg
2	ASIS breath	0.248	m
3	R. Thigh length	0.366	m
4	L. Thigh length	0.370	m
5	R. Mid-thigh circumference	0.470	m
6	L. Mid-thigh circumference	0.465	m
7	R. Calf length	0.372	m
8	L. Calf length	0.360	m
9	R. Calf circumference	0.322	m
10	L. Calf circumference	0.322	m
11	R. Knee diameter	0.098	m
12	L. Knee diameter	0.096	m
13	R. Foot length	0.0245	m
14	L. Foot length	0.243	m
15	R. malleolus height	0.072	m
16	L. Malleolus height	0.066	m
17	R. Malleolus width	0.063	m
18	L. Malleolus width	0.064	m
19	R. Foot breadth	0.090	m
20	L. Foot breadth	0.088	m

In order to drive the model to capture kinematics, motion agents were used. Motion agents were attached to the body segments with bushing elements. Their role is to track the trajectories of markers attached on the body and guide the model to follow the experimental kinematics. Motion agents are displayed on the model as small yellow spheres, their locations governed by the experimental data. The red spheres are fixed to the body segments of the scaled model. Yellow and red spheres are connected via the bushing elements (Fig. 2.6). The bushing stiffness of 100 N/mm and the damping coefficient of 10 N.sec/mm were considered for all directions.

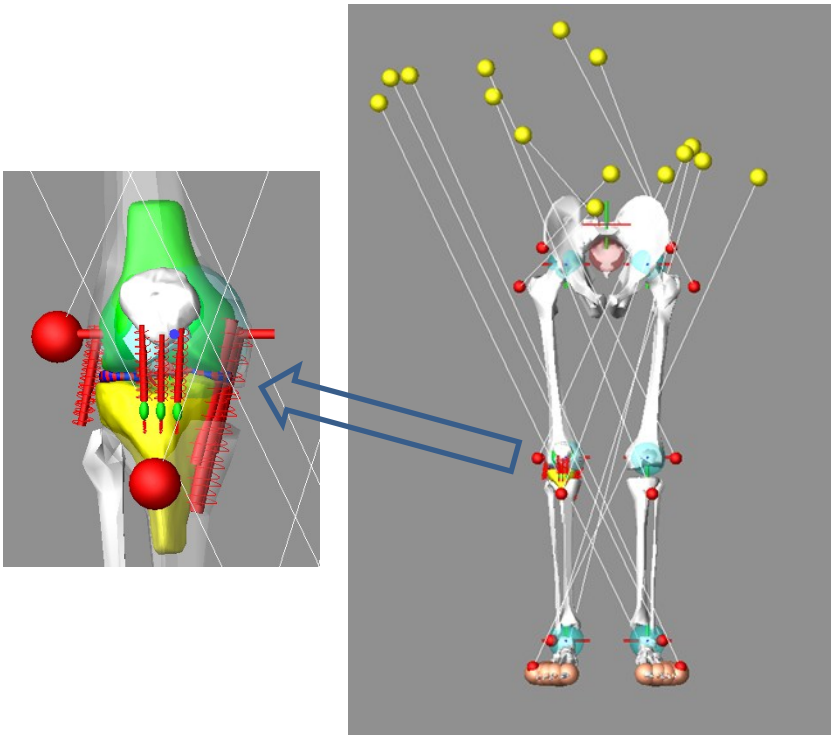

Figure 2.6: The developed multibody knee joint within the musculoskeletal model and creating the motion agents

2.4.1 Equilibrium Analysis

In order to fit the model to the first time frame of measured motion data, an equilibrium analysis was performed. In this step, motion agents (yellow spheres) were held stationary while the minimum energy configuration in the bushings was achieved (Fig. 2.7). After repositioning, the model posture was adjusted to the equilibrium position and then body marker locations (red spheres) and motion agents (yellow spheres) were synchronized. Next, forty-five muscle elements were placed on the right leg based on relative joint positions. The default attachments of the quad muscles were modified to insert on the patella (Fig. 2.7). While measured motion data drives the model in an inverse dynamics simulation, the muscle elements record their shortening/lengthening patterns. The elements repeat those patterns and serve as actuators for the forward dynamics simulation.

The interaction of the feet with the floor was simulated applying with ellipsoids-plane contact. The eleven contact ellipsoids, automatically created at the time of generating the model segments, were used to simulate the foot-floor contact (Fig. 2.8).

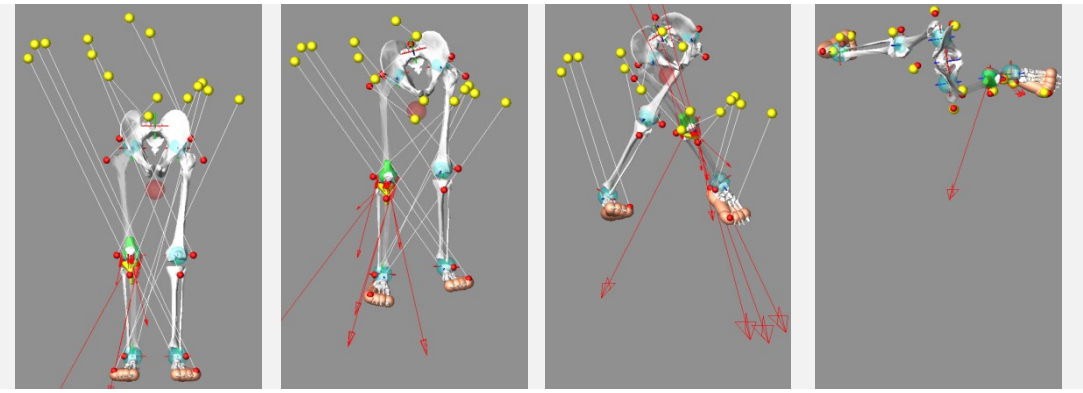

Figure 2.7: Moving the model to the equilibrium position based on the agent motion locations

The following parameters were considered for the foot-floor contact which was resulted in stable and realistic gait (Table 2.3).

Table 2.3
Foot-floor contact parameters

Stiffness	Damping	Exponent	Damping depth	Static friction
1.57 E-2 N/mm	0.35 Ns/mm	3	1mm	0.87

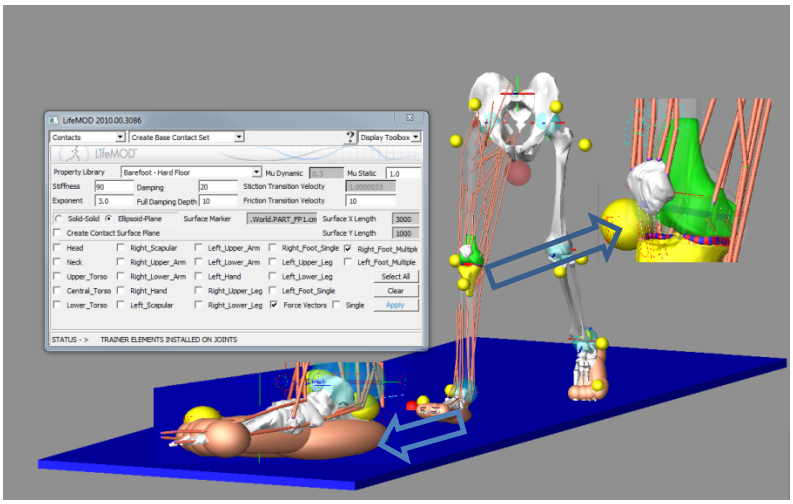

Figure 2.8: Adding 45 muscles and simulated ground reaction force

2.4.2 Inverse Dynamics

The measured motion data during the stance phase of the gait trial was used to run an inverse dynamics simulation. During this step, the red spheres, attached rigidly to the body segments, tracked the measured kinematics data via the motion agents (yellow spheres). However, these two spheres were separated (the bushings keep them united) when a discrepancy between the model performance and the measured motion data occurred (Fig. 2.9). This flexibility accounts for any error in data collections and measurements. The foot-floor contact was only created for the right leg, since during the stance phase the left leg was considered to be always off the ground and moving forward. As a result of the inverse dynamics simulation the rotations of the joints and the length of each muscle, through their respective via points, were recorded.

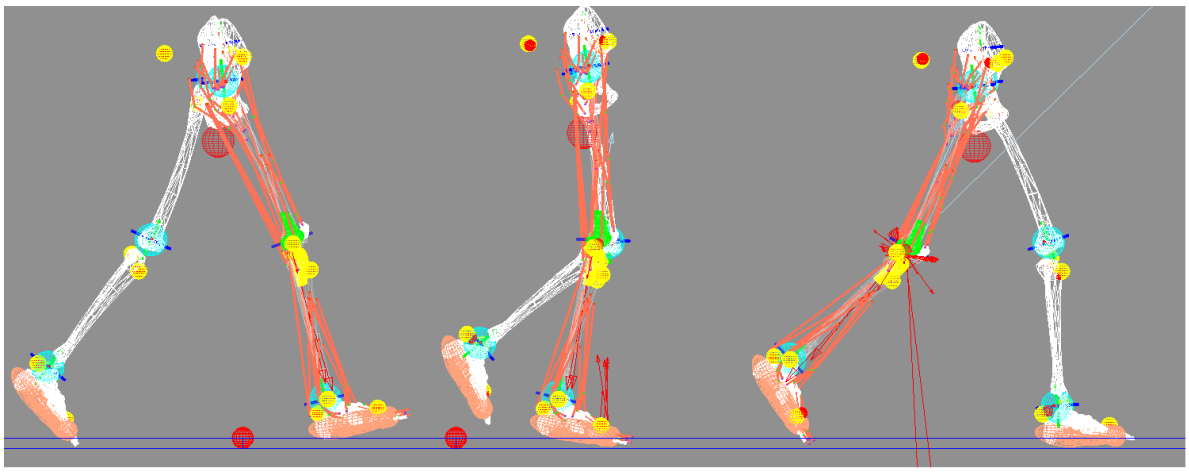

Figure 2.9: Inverse dynamics simulation

2.4.3 Forward Dynamics

With the recorded lengthening-shortening history of each muscle from the inverse dynamics simulation, muscle forces were generated to produce and recreate the motion history. Also all the joints for the left leg were trained to produce a torque to restore the left leg motion. This process involves removing the motion agents and updating the muscles and joints through feedback controllers.

Muscle parameters such as physiological cross sectional area (pCSA) and maximum tissue stress (σ_{max}) are used to calculate the maximum force potential of the particular muscle (Eq 2-6).

$$F_{max} = pCSA \times \sigma_{max} \tag{2-6}$$

LifeMOD™ contains a database of pCSA values for each muscle and is scaled accordingly based on the input body parameters (height, weight, gender and age). σ_{max} was 17.88 N/mm^2 for all muscles. The force generating capacity of each muscle was considered based on the proportional–integral–derivative feedback controller (PID). The PID controller algorithm uses the recorded muscle contraction as a target to generate the muscle activation. The governing equations of muscle forces are derived and given by:

$$F = P_{gain}(P_{error}) + I_{gain}(I_{error}) + D_{gain}(D_{error}) \tag{2-7}$$

Where:

$$P_{error} = \frac{target\ length - current\ length}{range\ of\ motion}$$

$$D_{error} = 1st\ derivative\ of\ P_{error}$$

$$I_{error} = time\ integral\ of\ P_{error}$$

The proportional gain was set to 1e5, Integral gain to 1e5, and derivative gain was set to 1e4. The maximum force generated by the PID controller was limited by the muscle maximum strength (Eq 2-6).

Proportional-derivative (PD) controllers were used to produce desired torques to recreate the motion history for each joint placed in left leg. The proportional gain was set to 1e+6 and the derivative gain was set to 1e+4.

Also a tracker agent was installed in order to guide the model and account for any dynamic instability. The tracker agent is a motion agent which is driven using the recorded inverse dynamic simulation [LifeModeler tutorial]. The passive translational spring stiffness and damping coefficient were selected 100 N/mm and 10 N.sec/mm while the torsional spring stiffness and damping coefficient were 1e+5 N.mm/deg and 1e+4 N.mm.sec/deg (Fig 2.10). In order to create the proper ground reaction force the tracker agent was specified free to move in the Superior-Inferior direction.

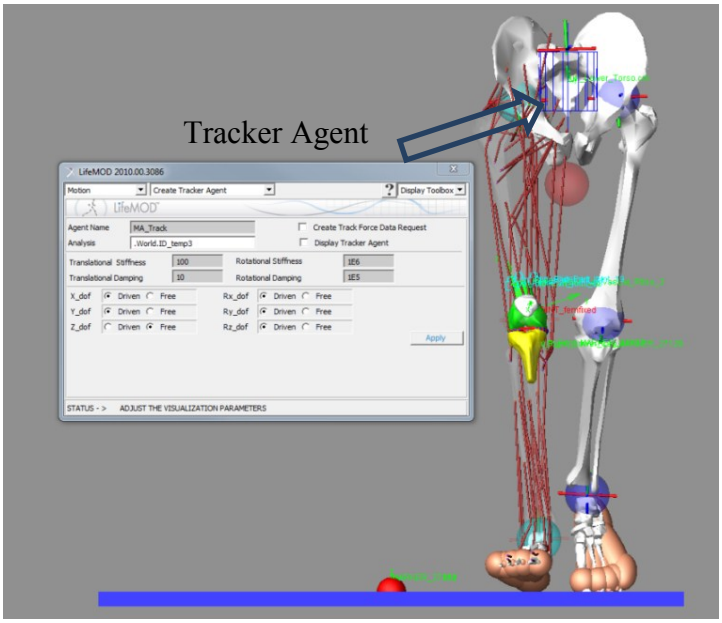

Figure 2.10: Tracker agent properties

Finally muscle driven forward dynamic simulations of the stance phase were run on two versions of the model (Fig 2.11). One version included representation of the menisci while in the second version the menisci were removed. Predicted ground reaction forces, muscle forces, tibio-femoral contact, ligament forces and hip/ankle joints orientations were recorded during the simulated walk cycle.

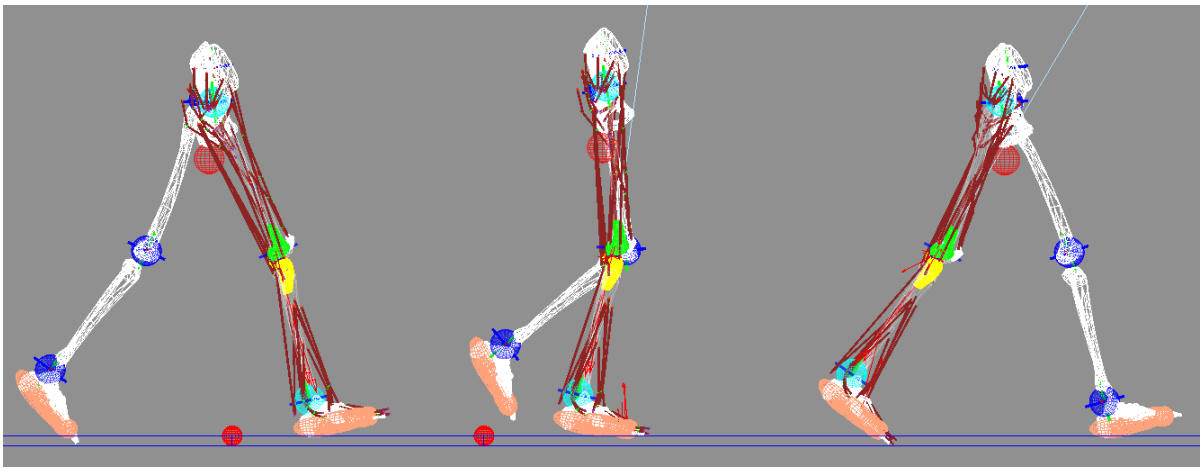

Figure 2.11: Forward dynamic simulation

CHAPTER 3

RESULTS

3.1. Meniscus Stiffness Matrix Parameters

As described in section 2.2.1, force–displacement relationships from Finite element simulations of a lateral and medial meniscus provided solution sets for optimization of spring matrix parameters connecting elements of lateral and medial multibody menisci models. Table 3.1 shows the stiffness matrix parameters of Eq. (2-1) prior to screening, after screening, and the final values after optimization. Also shown are the RMS errors between the Finite element displacement and Multibody displacement under 100N tensional load. The final RMS error was 0.017mm for the lateral meniscus and 0.051mm for the medial meniscus. Normalized RMS error was also calculated by dividing the RMS error by the finite element model range [Mishra M. 2010] and expressed as a percentage in Table 3.1. Lower percentage values show less residual variance and provide better fit.

Table 3.1
Spring matrix parameters , RMS errors and normalized RMS errors for the multibody meniscus models before screening, after screening, and final optimized values.

Parameter	Initial		After screening		Optimal	
	Lateral	Medial	Lateral	Medial	Lateral	Medial
K_θ (N/mm)	200	200	300	300	360	320
K_r (N/mm)	200	200	300	300	294	270
K_z (N/mm)	200	200	300	300	330	330
$K_{\theta r}$ (N/mm)	50	50	25	75	22.5	82.5
$K_{\theta z}$ (N/mm)	50	50	25	75	27.5	82.5
K_{rz} (N/mm)	50	50	75	25	75.5	25
T_θ (Nmm/rad)	50	50	75	25	67.5	25
T_r (Nmm/rad)	50	50	25	25	27.5	25
T_z (Nmm/rad)	50	50	75	25	71	22.5
RMS error (mm)	0.809	0.343	0.130	0.054	0.017	0.051
NRMS error %	42.6	17.6	6.93	2.78	0.90	2.62

3.2. Compliant Contact Parameters

A compressive axial load that linearly increased from 0 to 800N in 1 sec was applied to the distal tibia of the tibio-femoral finite element, and multibody models as well as tibio-menisco-femoral models. The resulting displacements at the load application point for the finite element and final multibody models are shown in Figure 3.1. The cartilage–cartilage contact parameters were determined by matching the three axes of translation (medial–lateral, anterior–posterior, and proximal–distal).

In order to facilitate the optimization procedure and concentrate on menisci primary function, the ability to dissipate compressive loads, only the proximal–distal displacement was used to fit the meniscus–cartilage contact parameters. Table 3.2 shows the final contact parameters for Eqs (2-2) and (2-3) along with values before and after screening. The RMS displacement errors and normalized RMS errors between the finite element and multibody models also are shown in table 3.2.

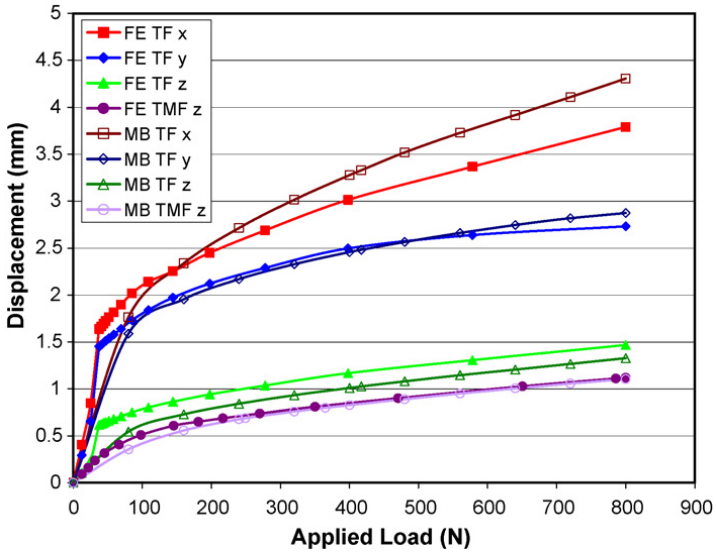

Figure 3.1: Displacement versus applied load for the finite element and multibody tibio-femoral models (TF) in the x (medial–lateral), y (anterior–posterior), and z (inferior–superior) directions and displacement versus applied load for the finite element and multibody tibio-menisco-femoral models (TFM) in the z (inferior–superior) direction.

Table 3.2
Parameters for the multibody compliant contact models and the resulting RMS error and calculated normalized RMS error between finite element and multibody displacement.

Parameter	Cartilage-Cartilage			Meniscus-Cartilage		
	Initial	After screening	Optimal	Initial	After screening	Optimal
K_c,K_m (N/mm)	500	250	327	37	18.5	19
B_c,B_m (Ns/mm)	5	7.5	5	1	0.1	0.1
exp_c,exp_m	1.5	2.25	2.07	1.5	2.25	3.37
RMS error (mm) medial–lateral	0.15	0.49	0.25	n/a	n/a	n/a
NRMS error %	3.94	12.9	6.57	n/a	n/a	n/a
RMS error (mm) anterior–posterior	0.32	0.23	0.12	n/a	n/a	n/a
NRMS error %	11.8	8.51	4.45	n/a	n/a	n/a
RMS error (mm) superior–inferior	0.27	0.08	0.13	0.27	0.08	0.04
NRMS error %	18.2	5.40	8.78	23.4	6.95	3.47

3.3. Multibody Knee Model Simulation

A subject specific Multibody model of the knee was placed in a Multibody model of a dynamic knee simulator and predicted tibio-femoral and patello-femoral kinematics were compared to measured kinematics from the cadaver knee exercised in the machine. Table 3.3 shows the RMS error and calculated normalized RMS error between simulated and experimental kinematics over one walk cycle in the knee simulator, for a model that included the multibody menisci and one that did not. A two sample t-test showed that there was no statistically significant difference in RMS error between the model with menisci and without menisci ($P > 0.05$). The position and orientation of the femoral, tibial, and patellar coordinates are defined by the attachment of the Optotrak system markers to the respective bones (Fig. 2.3). Figure 3.3 shows the position and orientation of the tibia marker relative to the femur for one walk cycle in the knee simulator, and Figure 3.4 shows the position and orientation of the patella. RMS errors between predicted and measured kinematics were generally low. The highest translational error occurred for the tibia in the femoral x-axis and was less than 11 mm (maximum range of motion was ~ 180 mm) and the highest orientation error occurred in the 3rd Euler angle sequence and was around 7° (maximum range of rotation was ~ 60°). .

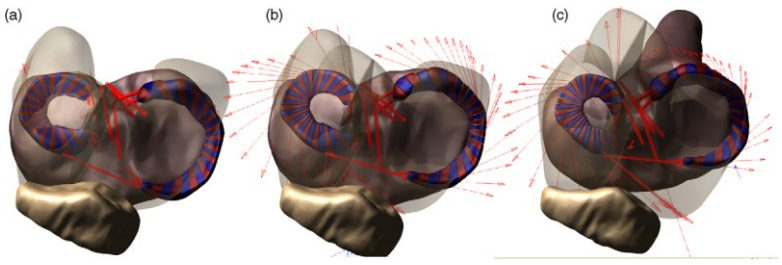

Figure 3.2: Simulation screen shots of the multibody knee model during a 10 s walk cycle in the knee simulator (**KKS)**. Shown is the tibial plateau at 0% of gait cycle (a), 20% of gait cycle (b), and 82% of gait cycle (c). The red arrows represent the resultant load on each spring matrix connecting the menisci elements.

Table 3.3
Calculated RMS errors and normalized RMS errors between prediction and measured kinematics for knee models with and without inclusion of the menisci.

	Tibia						Patella					
	Translation (mm)			Orientation (deg)			Translation (mm)			Orientation (deg)		
	x	y	z	1	2	3	x	y	z	1	2	3
With meniscus RMS error	10.3	5.00	2.80	1.40	1.60	6.80	1.90	4.60	6.50	3.80	2.60	6.30
NRMS error %	20.6	6.25	1.60	2.26	8.88	68.0	9.50	11.5	18.6	16.5	21.6	57.3
Without meniscus RMS error	10.6	6.60	2.90	2.10	2.20	6.30	2.10	4.60	7.30	3.70	2.60	6.40
NRMS error %	21.2	8.25	1.65	3.39	12.2	63.0	10.5	11.5	20.8	16.1	21.6	58.2

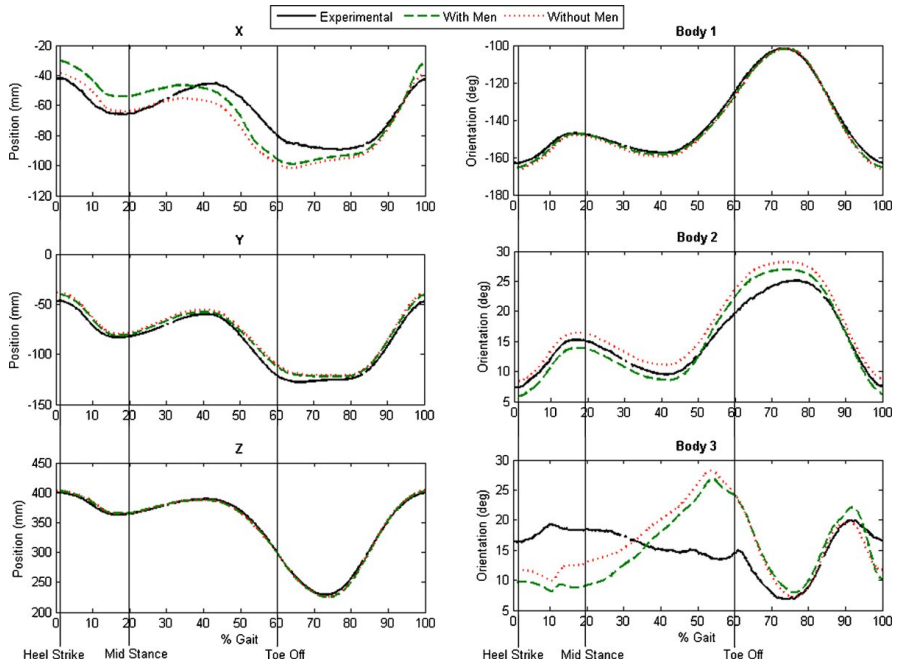

Figure 3.3: Position (x,y,z) and orientation (body 1,2,3 Euler sequence) of the tibia coordinate system relative to the femoral coordinate system for one walk cycle (KKS).

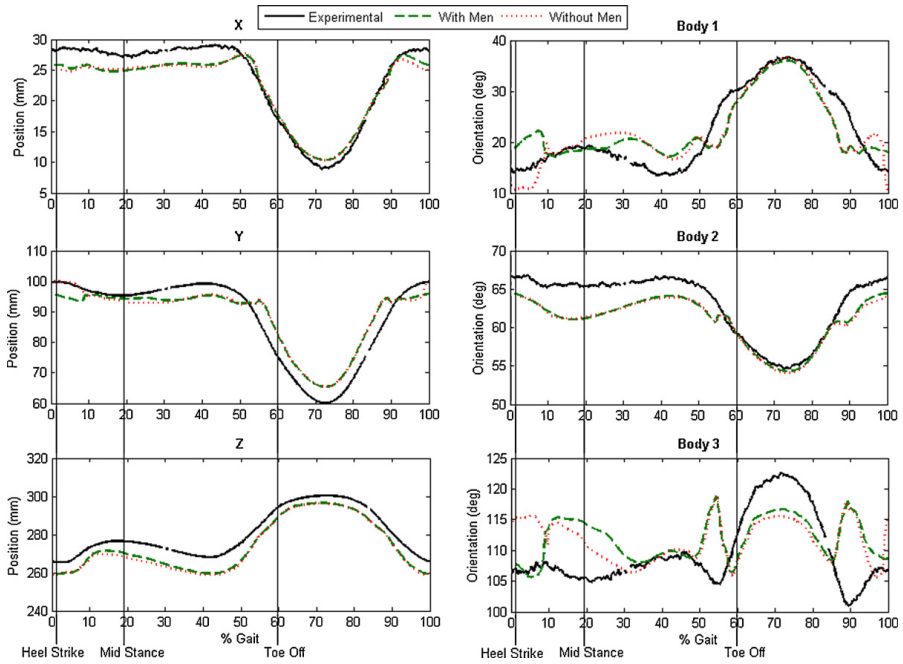

Figure 3.4: Position (x,y,z) and orientation (body 1,2,3 Euler sequence) of the patella coordinate system relative to the femoral coordinate system for one walk cycle (KKS).

3.4. Contact forces

The RMS error (normalized percentage RMS error) between predicted quadriceps force and measured quadriceps force was 130N (9.84%) for the model with the menisci and 121N (9.16%) for simulations without the menisci (Fig. 3.5). The small difference observed in calculated RMS errors may be explained as a result of computational errors and complexity in the model with menisci. Table 3.4 gives the maximum predicted tibio-femoral contact force for the medial and lateral condyles for models with and without the menisci. Contact forces over the entire modified walk cycle are shown in Figure 3.6. The addition of the menisci to the model significantly reduces contact between the tibia cartilage and femur cartilage for the lateral side (two sample t-test $P < 0.05$). On the medial side, the addition of the menisci was not statistically significant. Figure 3.7 provides the contact force between each meniscus element (28 lateral and 32 medial) and the tibial plateau. The highest contact force for a single element is 43N on the lateral side and 23N on the medial side.

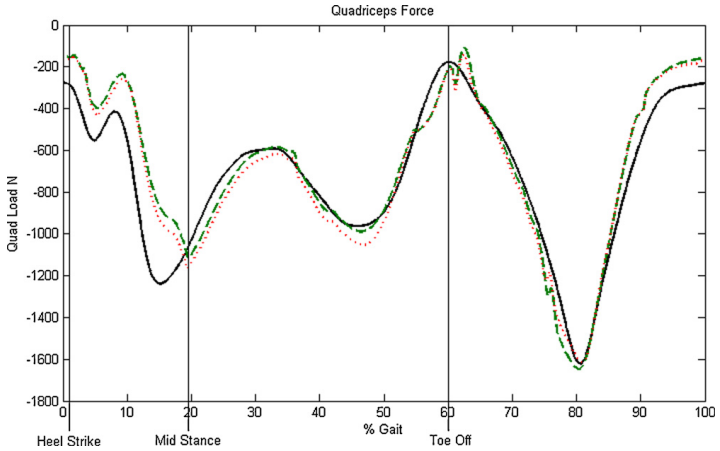

Figure 3.5: Predicted (with menisci (- - -) and without menisci (· · ·)) and measured (—) quadriceps force over one walk cycle (KKS).

Table 3.4
Contact force predicted by the tibio-femoral compliant contact model for models with and without the menisci.

	With menisci		Without menisci	
	Lateral condyle	Medial condyle	Lateral condyle	Medial condyle
MAX contact force	632 N	1755 N	937 N	1735 N
% gait cycle at max contact	81%	48%	82%	50%

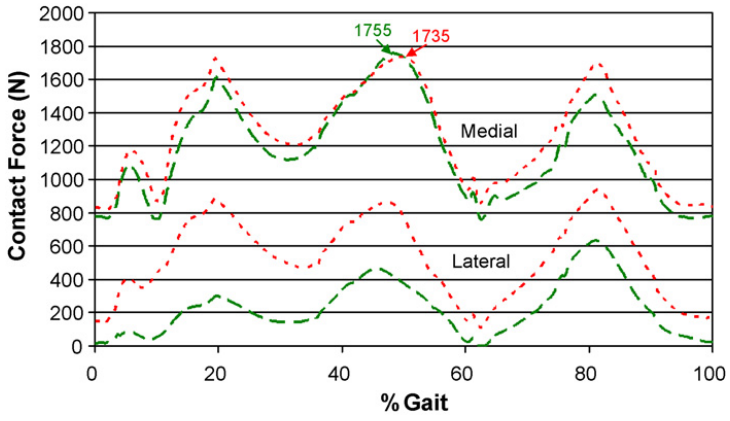

Figure 3.6: Predicted tibio-femoral contact forces for a model with menisci (- - - -) and without menisci (….) over one walk cycle (KKS).

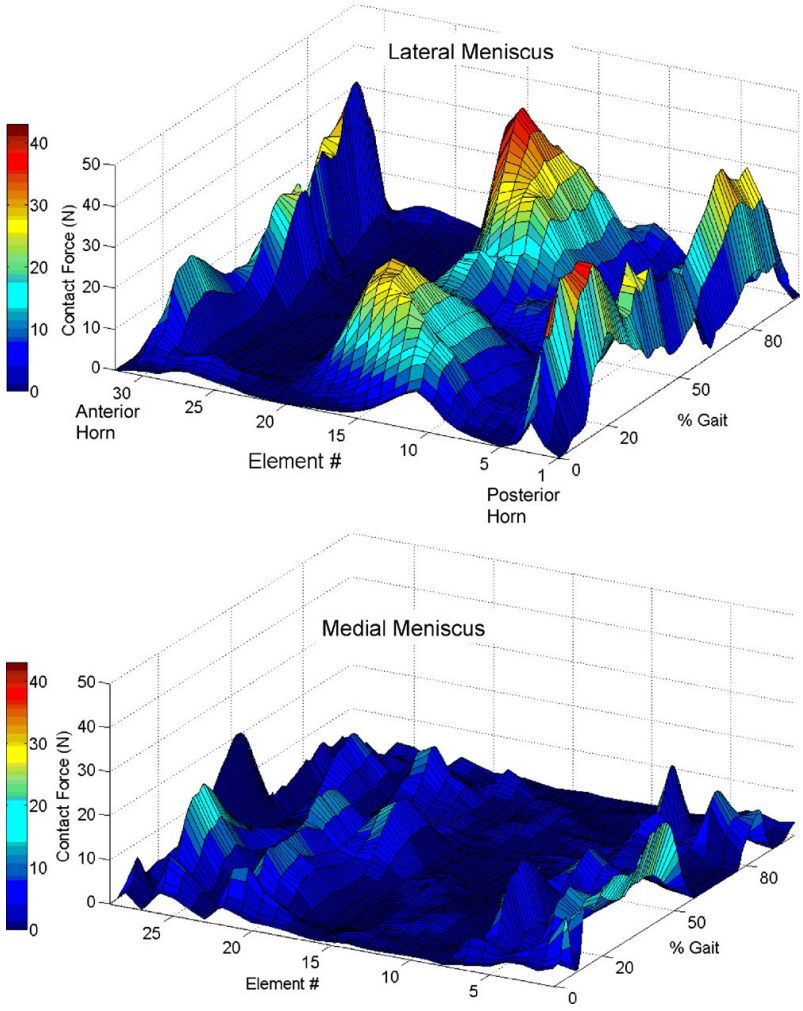

Figure 3.7: Force predicted by the compliant contact model between each meniscus element and the tibia during a walk cycle (KKS). Element 1 connects at the anterior horn and element 31 (lateral) and 29 (medial) connect at the posterior horn.

3.5 Musculoskeletal Model Simulation Results

The comparison between the predicted ground reactions forces with experimental data reported in reference [Vaughan CL. et al. 1999] are illustrated in Figure 3.8. The simulated ground reaction forces were passed through a 3rd order butterworth low pass filter with a cutoff frequency of 6Hz, the same as experimental. As illustrated in the Figure 3.8, the predicted forces show a good agreement with the experimental values during the stance phase of the walk cycle.

The calculated root mean square errors (normalized percentage RMS error) were 72.6 N (10.2%), 22.6N (44%), and 31N (11%) for the Z (Superior-Inferior), Y (Lateral-Medial) and X (Anterior-Posterior) directions respectively.

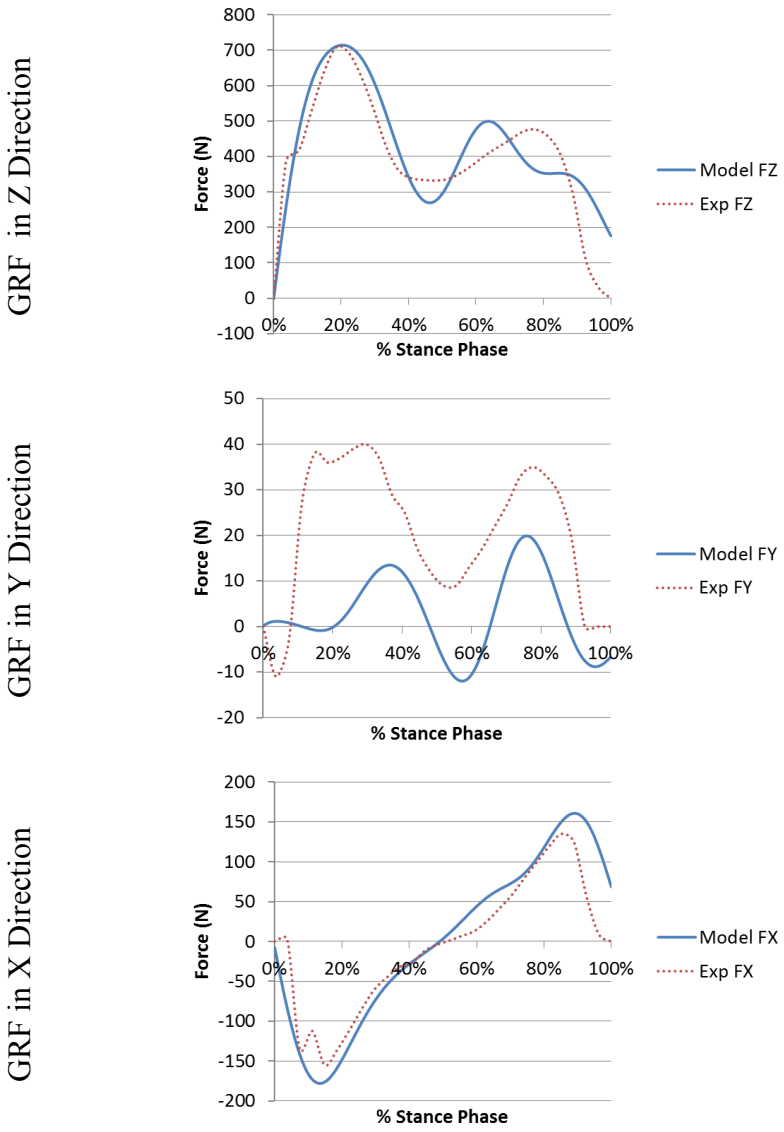

Figure 3.8: Predicted ground reaction forces compared to the experimental data

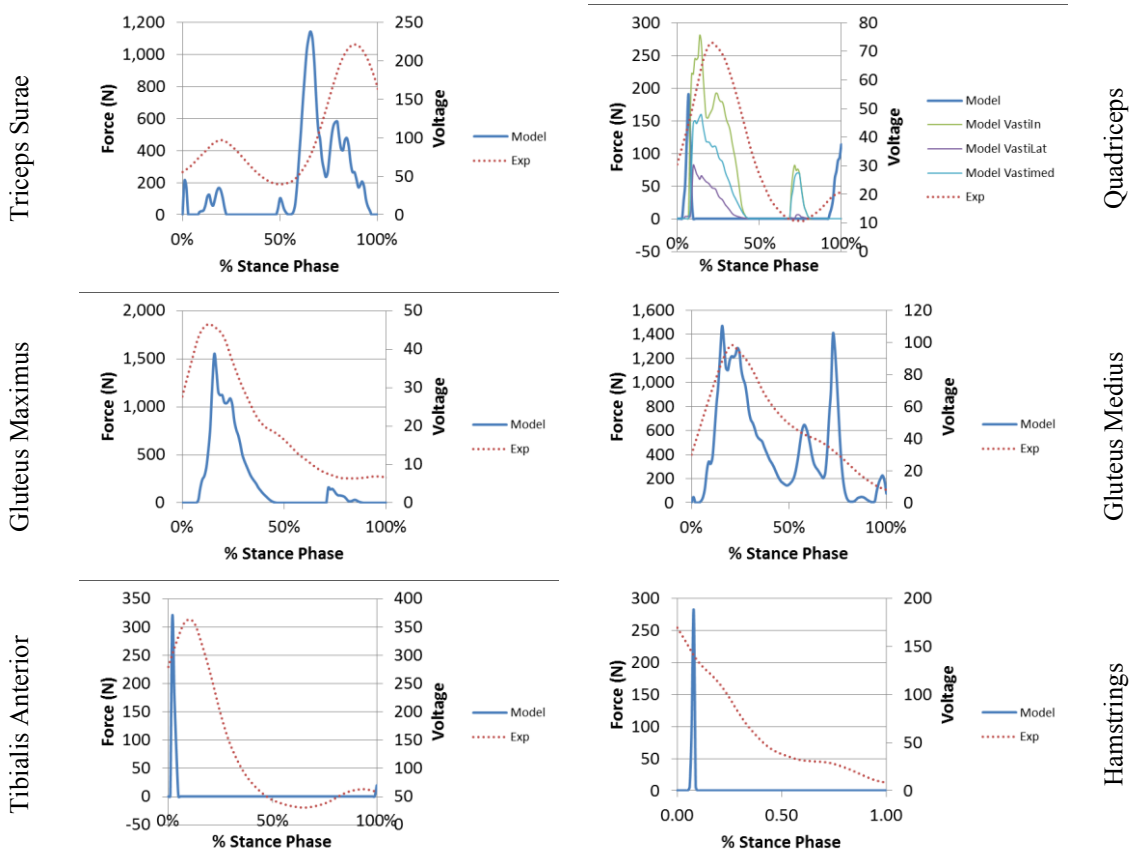

Figure 3.9: Model predicted muscle forces and experimental filtered surface EMG

Figure 3.9 provides force predictions for the major muscles of the lower extremity as well as their measured filtered electromyography (EMG) data. EMG signals were full-wave rectified, and smoothed using a low-pass 2nd order Butterworth filter with a cut-off frequency of 3Hz [Olree K. and Vaughan CL. 1995]. Illustrated in Figure 3.10, gluteus medius, gluteus maximus, rectus femoris, hamstrings, tibialis anterior, and gastrocnemius were selected for the surface EMG analysis [Olree K. and Vaughan CL. 1995].

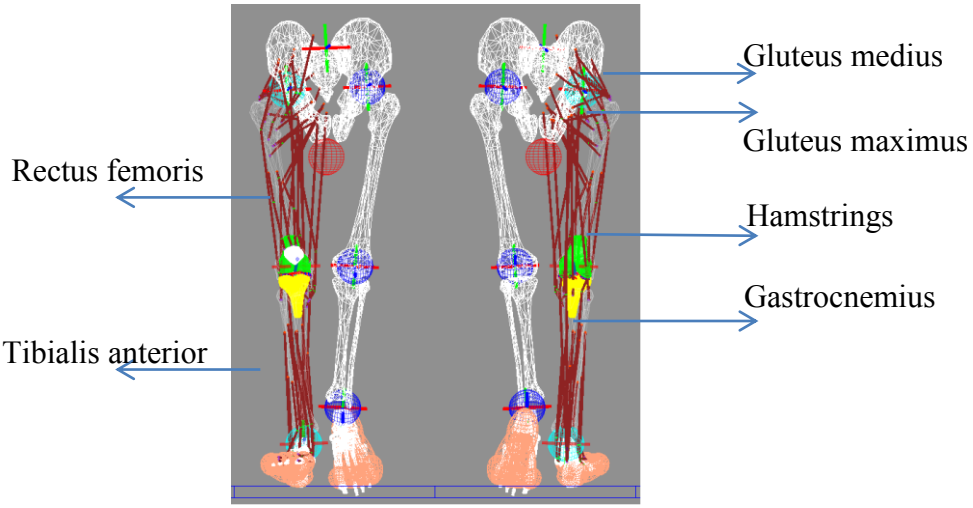

Figure 3.10: Major muscle groups were selected for comparison

In general, the predicted muscle forces followed measured muscle activation patterns. During the initial loading response (heel strike), the gluteus medius, gluteus maximus , quadriceps (rectus femoris and vastus group) and hamstrings supplied the majority of muscle forces to oppose the hip flexion and provide stability at the knee joint (Fig. 3.11). This assumption is valid since the measured EMGs have shown that these muscles are activated at the beginning of the stance phase. Directly after contralateral toe-off (when the left leg leaves the ground) the quadriceps group acts to extend the knee therefore these muscles are activated during mid-stance. In contrast, the gastrocnemius acts during the late-stance to flex the knee while creating an ankle plantar flexion (Fig. 3.11).

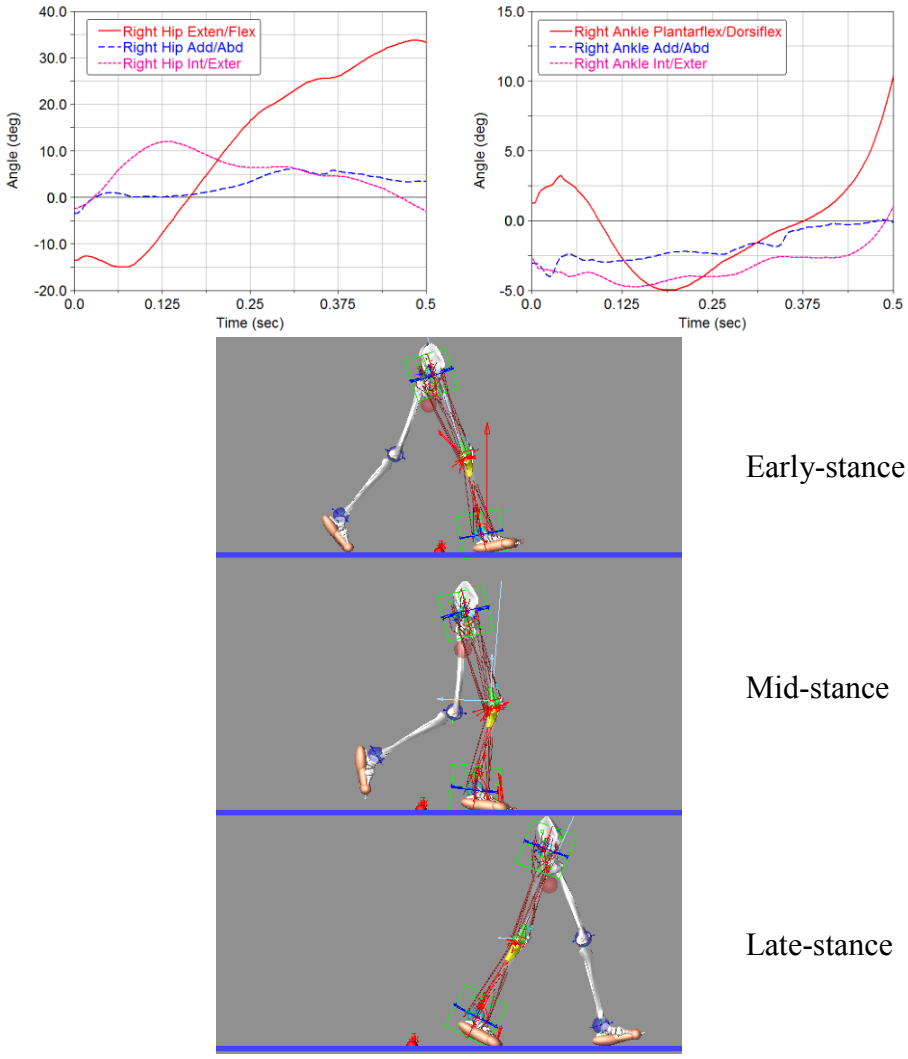

Figure 3.11: Hip and Ankle joint rotations during heal strike, mid-stance, and late-stance of the walk cycle

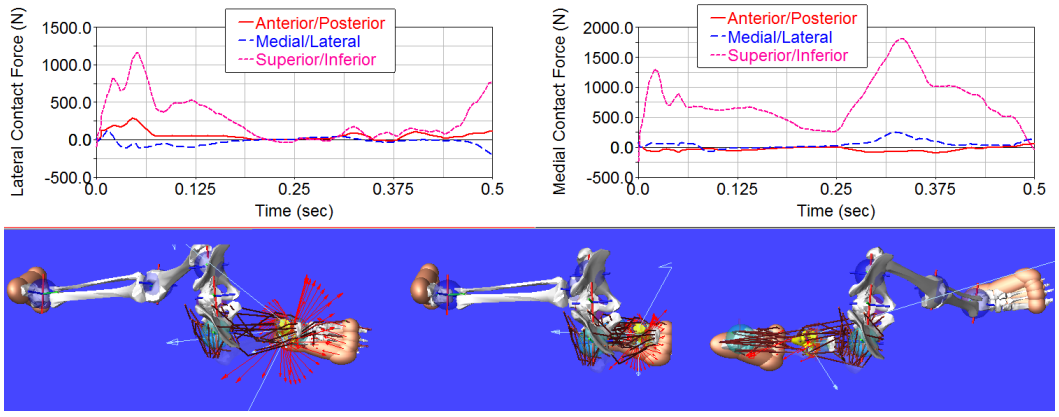

Figure 3.12: Predicted lateral and medial contact forces on femoral condyles

Predicted lateral and medial contact forces are presented in Figure 3.12. The predicted results show that the total distributed force was concentrated on the medial component of the femoral cartilage. Furthermore, the total tibio-femoral contact force shows the familiar "double-bump pattern", with first bump occurring after opposite toe-off and the second bump occurring prior to opposite heel-strike (Fig. 3.13). The average and maximum total contact force across the knee joint were predicted 2.7 BW and 5.3 BW (person body weight was 510 N) respectively.

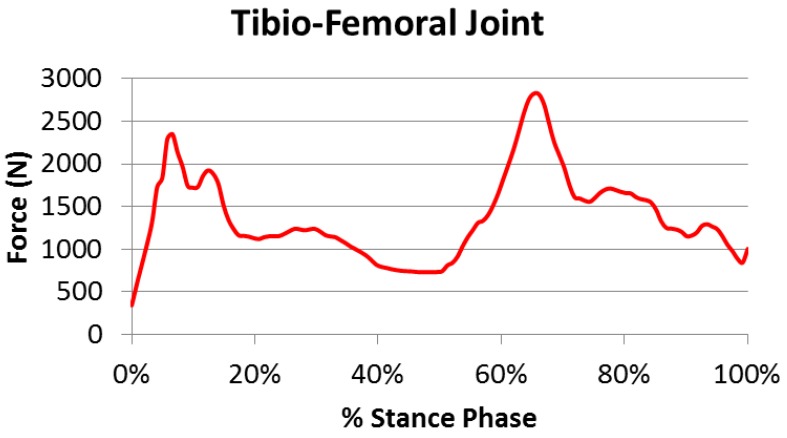

Figure 3.13: Total contact force on tibio plateau during the stance phase of gait

Figure 3.14 provides pictures of the tibia plateau and menisci looking through the femur, at three different time steps during the simulation. As it has been illustrated(Fig. 3.14), at the beginning of stance phase, while the knee flexes, the menisci geometries move posteriorly and then immediately after opposite toe-off they start to move anteriorly. This observation is in agreement with the study by Vedi et al. (1999) on menisci movements.

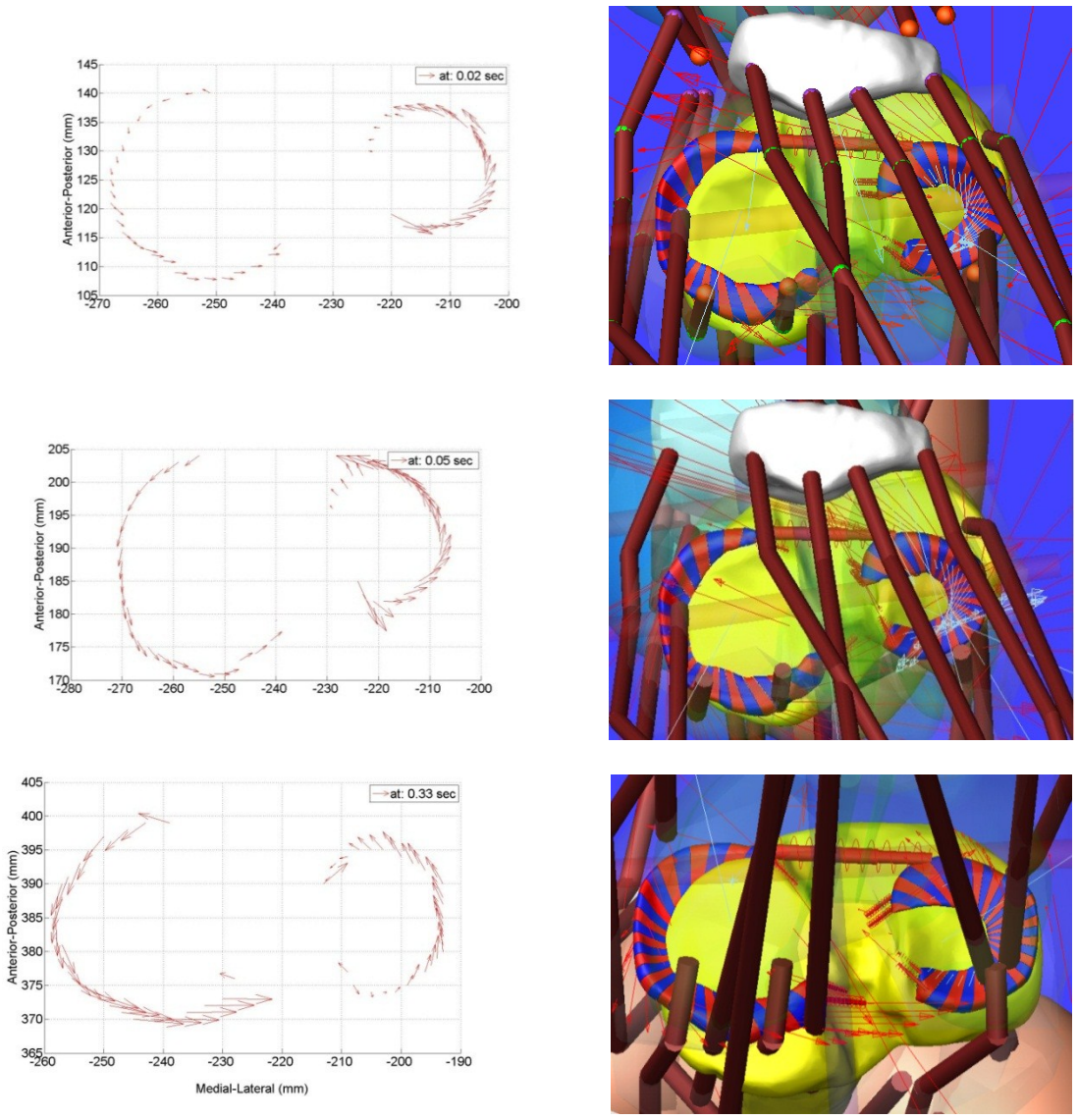

Figure 3.14: Load distribution in the medial and lateral meniscus with their deformation during the gait

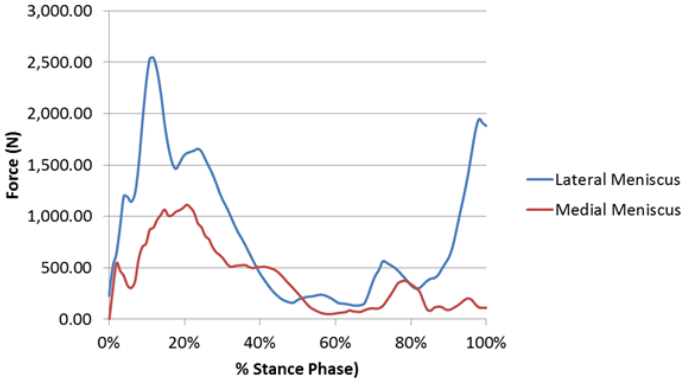

Figure 3.15: Total circumferential tension force for each meniscus

The difference in the circumferential tension within menisci was also compared between the lateral and medial meniscus (Fig. 3.15). During the early stance, both menisci were experiencing their maximum tension. The maximum tension force was approximately 2 times greater in the lateral side than medial side. The difference might be explained by a defected structure observed in the medial meniscus (Fig. 3.16). This degeneration caused uncontrolled movements and loss of menisci functionalities in the medial side. As a result, during the simulation the medial meniscus did not conform well to its respective tibial and femoral articulation surfaces therefore provided minimal load distribution.

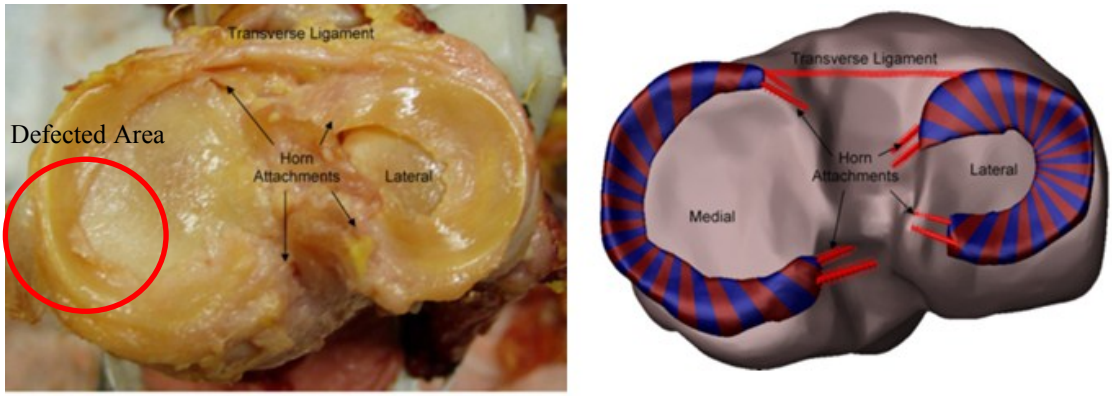

Figure 3.16: Picture of the menisci and tibial plateau for the cadaver knee and model

Ligament forces during the stance phase of gait were also calculated (Fig 3.17). As discussed in section 2.2.4, the origin and insertion sites of different ligaments were determined from MRI and point clouds obtained by physically probing the cadaver knee. The net forces in respective ligaments were the result of adding up all individual bundles.

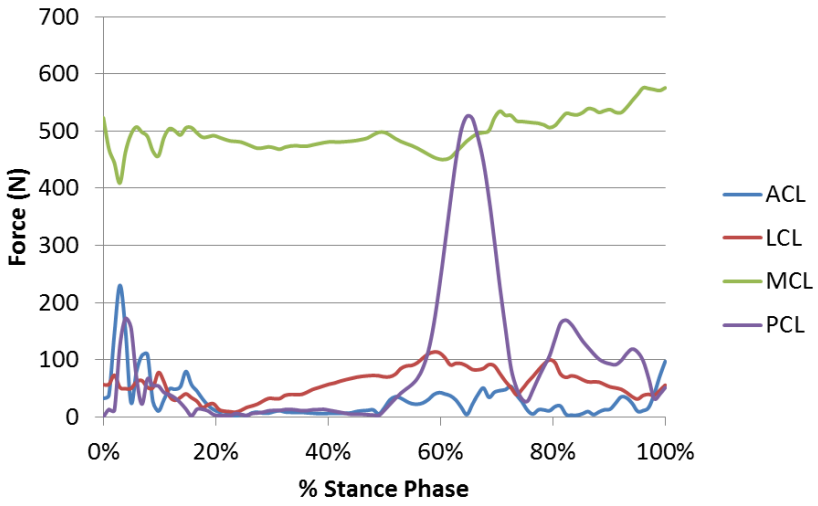

Figure 3.17: Ligament forces during the stance phase of the gait

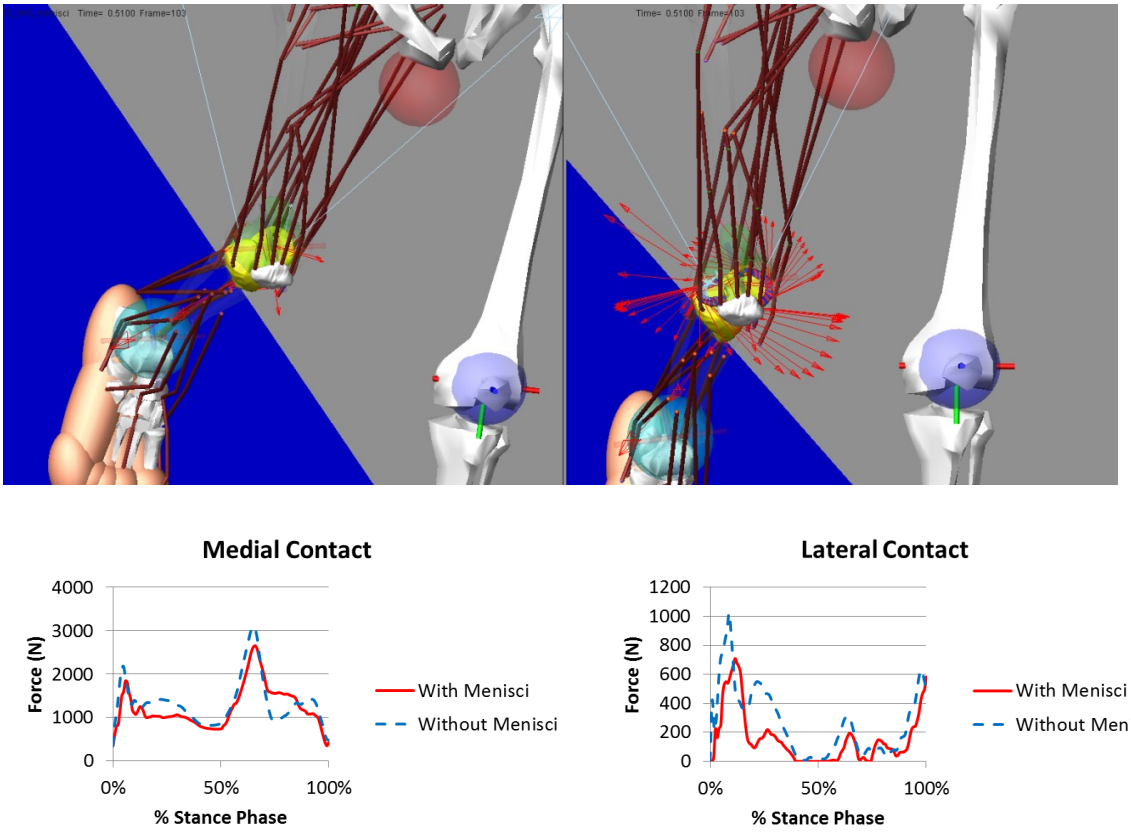

Figure 3.18 : Comparison of predicted magnitude of medial and lateral contact forces in the model with menisci and without menisci

Total contact forces on the medial and lateral tibia plateau for simulation with and without menisci are shown in figure 3.18. As it can be seen, inclusion of menisci provides a significant reduction in peak contact force on the lateral tibia articular cartilage. At the early-stance, the lateral peak contact force is 1021 N for a simulation without menisci and 655 N with menisci. In contrast, removing the menisci did not change the force significantly on medial side. Figure 3.18 also shows the knee joint during the simulation for the model with and without menisci.

Figure 3.19 and 3.20 show a comparison of the hip and ankle joint orientations during the inverse and forward dynamics simulations, for the case with and without menisci. Results indicated that the addition of the menisci improved the forward dynamics prediction on tracking desired trajectories of anatomical joint angles. Table 3.5 shows the calculated root mean square (RMS) error of the predicted hip/ankle orientations between the forward dynamics predictions and inverse dynamics one. The normalized root mean square error was also calculated as a ratio of RMS error to the range of motion for the model with menisci and without menisci.

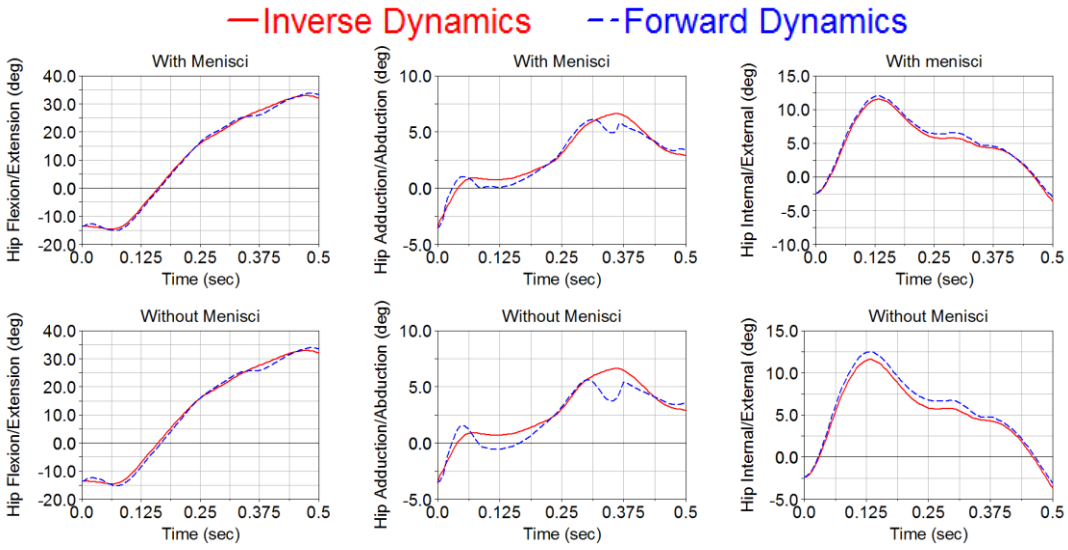

Figure 3.19: Hip orientations over the stance phase of the gait cycle

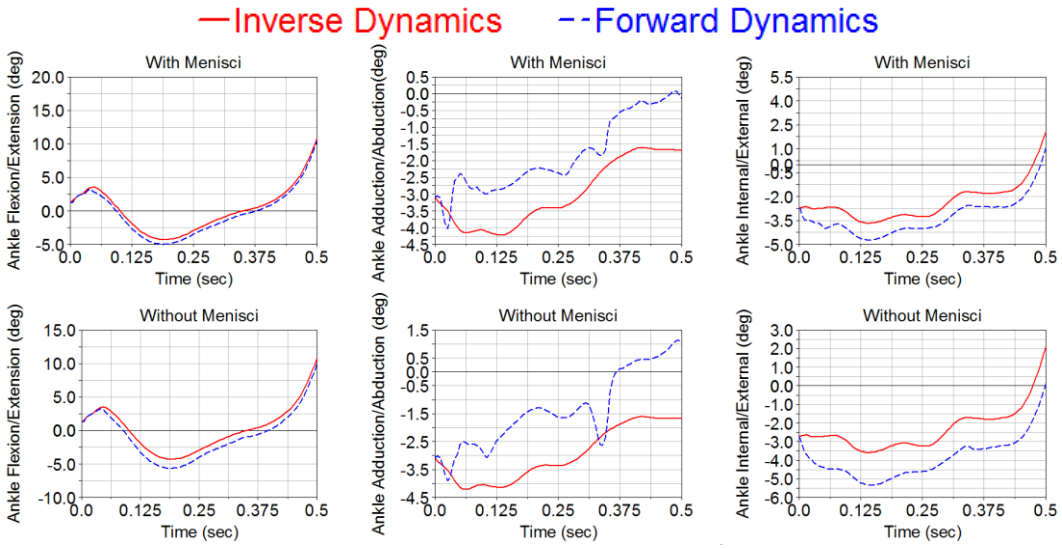

Figure 3.20: Ankle orientations over the stance phase of the gait cycle

Table 3.5
Calculated root mean square error (RMS error) and the percentage of normalized root mean square error (NRMS error) for the hip and ankle joints orientations

		Hip			Ankle		
		Flexion Extension	Adduction Abduction	Internal External	Flexion Extension	Adduction Abduction	Internal External
RMS error	With Menisci	0.74deg	0.59 deg	0.44 deg	0.57 deg	1.24 deg	0.95 deg
	Without Menisci	1.05 deg	1.00 deg	0.70 deg	1.04 deg	1.78 deg	1.60 deg
NRMS error	With Menisci	1.56 %	9.38 %	2.7 %	3.34 %	46.00 %	14.40 %
	Without Menisci	2.21%	15.89 %	4.33 %	6.00 %	67.00 %	24.26 %

Ligament forces were recalculated for the simulation without menisci and compared to the model with menisci (Fig 3.19). Only anterior cruciate ligament (ACL) force increased significantly after removing the menisci. The predicted average forces during the stance phase for all ligaments are reported in table 3.6.

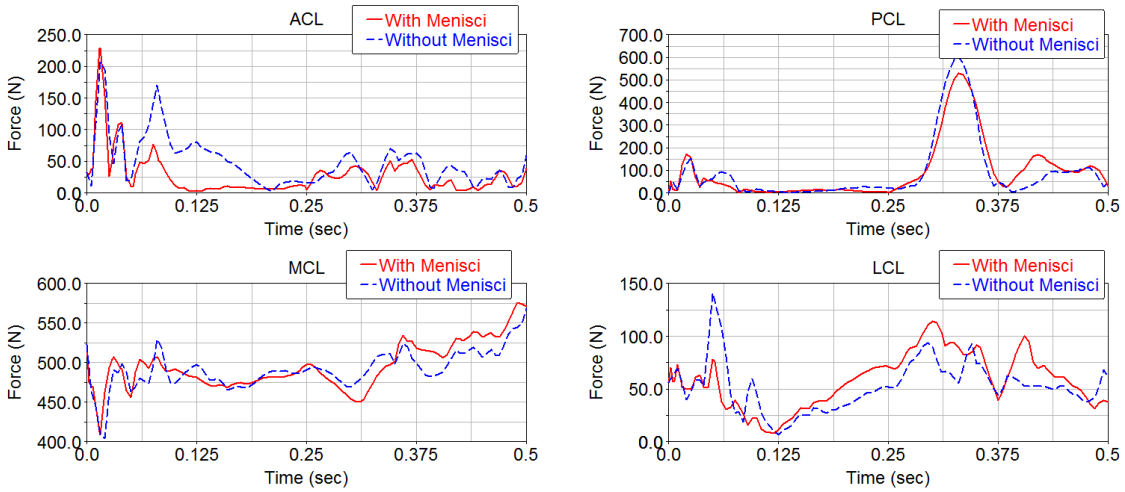

Figure 3.21: Comparison of ligament forces

Table 3.6
Average forces predicted in the knee ligaments during the stance phase of gait for the case with inclusion of the menisci and without of the menisci

	ACL	PCL	MCL	LCL
With Menisci	29.8 N	88.0 N	496.0 N	58.5 N
Without Menisci	48.0 N	90.1 N	491.7 N	52.2 N

3.5. Simulation time

The computational time for the multibody tibio-menisco-femoral model was 30 s of computation time for each second of simulation time (0.01 s step size, default ADAMS solver, desktop PC (Dual Core 5160 Xeon Processor (3 GHz) with 2GB of RAM)). And the computational time for the musculoskeletal model with 45 muscles with inclusion of a detailed model of the knee with menisci was 178 second (0.005 s step size, contacts optimized ADAMS solver, desktop PC (Intel® Xeon® Processor (3 GHz) with 9GB of RAM)).

CHAPTER 4

DISCUSSIONS

The motivation for this work was to develop dynamic 3D anatomical knee models that have a computational efficiency sufficient for incorporation in forward dynamics movement simulations. Presented here is a method to represent the menisci within a multibody framework and study their motions and functionalities in a musculoskeletal model.

It has been shown that inclusion of the menisci provides a small improvement in kinematics and a significant difference in the distribution of tibio-femoral loading during activates. This may indeed suggest that the menisci should be included in investigations where cartilage loading is important.

In order to measure the model accuracy, the root mean square error (RMS error) and the normalized root mean square error (NRMS error) were reported. Usually a model with small RMS and NRMS errors is considered to be “good”. Although, there is no absolute criterion for a “good” value of normalized RMS error, in this study predictions with normalized RMS error less than 20% were considered to have a good agreement with the values observed from experiments.

In the first step the knee model where loaded by placing it within a model of a dynamic knee simulator. This was an intermediary step in model development that facilitates model validation as the forces applied to the knee simulator were known and bone motion could be directly measured. This method demonstrated that during the simulated walk cycle in the knee simulator, the menisci provide only a secondary kinematic constraint. Although the simulated walk cycle was based on ISO specification 14243-1:2002, it was modified and slowed to 10 sec because of technical limitations. A typical walk cycle is approximately 1 sec. The predicted peak contact force without the menisci was 937N at 82% gait for the lateral condyle and 1735N at 50% of gait for the medial condyle. The maximum contact force for the lateral condyle occurs during the swing phase of stance. This high compressive load during swing was due the high force from the quadriceps actuator required to extend the knee in the dynamic knee simulator (Fig. 3.5). The developed knee model had accurate prediction of the tibio-femoral motion, patello-femoral motion, and quadriceps force of the cadaver knee loaded in the dynamic knee simulator (normalized RMS error less than ~ 20%). But, the accumulated orientation errors in the Euler sequence prevented accurate prediction of tibio-femoral and patella-femoral 3rd rotations (normalized RMS error greater than 50%).

Since the kinematics and quadriceps force were replicated accurately by the model, it is believed that the predicted contact forces were representative of the contact forces of the cadaver knee during the walk cycle in the knee simulator. However, this could be verified if the experimental measured force was available.

Inclusion of the menisci significantly reduced tibio-femoral contact forces on the lateral side. But, meniscus inclusion did not show a significant reduction on the medial side,

even slightly increasing the maximum contact force. The cadaver knee was from a 78-year-old female and the medial meniscus only covered the outer periphery of the tibial plateau (Fig. 3.16). During simulation, the medial meniscus did not conform to the medial femoral condyle and only provided minimal load transfer. It is possible that a decrease in the size of the menisci with age could be a significant factor in development of osteoarthritis.

A macro was written to automatically divide the MRI derived geometries of the menisci, assign material properties, and define contacts with neighboring cartilage. Properties for 6×6 spring matrices connecting the menisci elements and deformable contact parameters for the cartilage–cartilage and cartilage–meniscus contacts were derived from a Finite Element solution [Mishra M. 2010]. However, this could be improved through designing an experiment to measure contact forces directly, for example through pressure paper placed between the meniscus and tibial plateau, or determine meniscus displacement under a semi-physiological loading condition [Paiva G. 2010].

The final goal of this study was to incorporate the developed knee model within a lower extremity musculoskeletal model and simulate the knee kinematics during the stance phase of a gait cycle (approximate simulation time was 0.5 sec). The musculoskeletal model was capable of predicting ground reaction forces, muscle and ligament forces as well as tibio-menisco-femoral contact mechanics.

As it can be seen in Figure 3.1, the predicted ground reaction forces during the stance phase followed the experimentally measured forces very well (normalized RMS error of ~ 10%), with the exception of 2nd peak seen in the vertical force. Traditionally a “double bump pattern” is presented for the vertical ground reaction force. The 1st peak is associated with

deceleration during heel-strike and the 2nd with acceleration during push-off [Nigg M. and Herzog W. 2007].

As it is described in section 2.4.1, in the current study the foot model was consisted of eleven ellipsoidal surfaces to simplify the foot-floor contact model. This simplification might also explain the higher normalized RMS error observed in medial-lateral direction (~ 40%). It is believed that replacing an anatomical model of foot or shoes with the simple ellipsoids would provide a better force prediction. Also the metatarsophalangeal joint was ignored in the current study. It has been shown that the metatarsophalangeal joints affect the foot motions specifically during push-off [Zatsiorsky VM. 1998].

Predictions of the muscle activation timing from the feedback control approach had a good agreement with measured EMG. However the disadvantage of this method is that they do not adequately predict the co-contraction of antagonistic muscles during gait. The use of more sophisticated models of muscle such as Hill-models could recover this weakness.

The predicted lateral and medial knee contact force (Fig. 3.12) indicated that the medial compartment of the knee joint is experiencing much larger forces compare with the lateral compartment. This observation may explain why osteoarthritis occurs more often in the medial compartment of the knee joint than lateral compartment.

The predicted tibio-femoral contact force on an instrumented prosthetic knee during the gait was provided in several literatures [Zaho D. et al. 2007, Kim J. et al. 2009]. For example Zhao D. et al. (2007) reported a peak contact force of ~670N at 20% gait cycle for the lateral contact and a peak contact force of ~800N at 50% gait cycle on the medial side of a knee implant. In a similar study, Kim J. et al. (2009) predicted tibial contact forces for three different walking speeds from a single male patient (80 years old, and a body weight of

68 kg). The total maximum calculated knee load was about 2.7 BW and it occurred during the late-stance.

Due to the fact that the subject for the musculoskeletal model was different than the cadaver based anatomical knee, the maximum total force in current study was much larger than those seen in previous studies. In addition, a large predicted gastrocnemius force at the end of mid-stance (~ 60% of stance phase) flexes the knee prior to the opposite heel-strike which the corresponding peak in the tibio-femoral force also occurs at this time.

It is believed that the forces acting on knee joints are dependent on the muscle forces crossing the joint and developed ground reaction forces [Kim J. et al. 2007]. Therefore any improvement in estimation of these forces would provide a better prediction.

Menisci movements were well described in Vedi V. et al. (1999) study. They used an "open" magnetic resonance scanner to scan an intact in vivo knee under load in all different positions. Using such a scanner, they observed that the menisci move posteriorly as the knee flexes and the lateral meniscus is more mobile than the medial meniscus. Figure 3.14 indicates a good agreement with this experimental report.

In order to prevent the meniscus from extruding out of the joint, under the compressive tibio-femoral force, internal forces act circumferentially inside the meniscus shown in Figure 3.14. This provides the menisci functionality to support the knee while the load is applied over the knee joint. The maximum circumferential forces were 2500 N for the lateral side at ~ 11% of the stance phase and about 1080 N for the medial side at ~ 20% of the stance phase. These results, however, have not been verified since there are no published studies investigating similar conditions

The magnitude of the ligament forces calculated in the current study is depicted in figure 3.17. The material properties of the ligaments were taken form cadaver based study, presented in section 2.2.4. The largest forces occurred in the MCL and PCL. The maximum force in MCL was approximately 576 N at 96% of the stance phase. The maximum force of 526 N occurred in the PCL, approximately at mid-stance, to provide resistance to the tibia rotation. Although the maximum forces were larger compared with other published studies [Morrison JB. 1970, Yang NH. et al. 2010], Morrison (1970) notes that the forces in knee ligaments can vary significantly between individuals due to subject specific gait characteristics and knee joint geometries. The limitation of using cadaveric knee geometry along with gait data from a similar size female may also contribute to the larger ligament forces.

Finally exclusion of the menisci increased the average tibio-femoral contact forces by 67% and 9% on the lateral and medial side respectively. In addition, during the forward dynamics simulations, tracking the desired trajectories of anatomical joints was improved by preserving the menisci in the model. Table 3.5 indicated that the calculated RMS errors and the normalized RMS errors were increased by removing the menisci. Therefore, in contrast to the early results from the knee simulator model, it has been shown that the menisci had a kinematics constraint function in the knee joint. A comparison between these two models may suggest that it is essential to have a realistic walking pattern and simulation to obtain a most realistic prediction of the soft tissues behaviors. However, not much change has been seen in ligament forces after removing the menisci, with the exception of ACL (the average force in ACL increased by 60%). These results clearly demonstrated menisci functionalities as a load distributor as well as kinematics constraint in the knee.

Almost all musculoskeletal models, whether based on inverse dynamics or forward dynamics, are implemented using a multibody framework. Generally the development time of the multibody models is much faster than development and meshing time of the finite element models. In presented study, the computational time to solve the inverse and forward dynamics problems were less than 10 minutes. Although no attempt was made to optimize computation time of the multibody model via meniscus element size, solver settings, parallel processing, or other means, it is believed that the computation time of the model could be significantly reduced.

In summary, the limitations of this study include: (1) concentrating only on the stance phase of a walk cycle and ignoring the swing phase, (2) using a cadaveric knee geometry along with gait data from a subject with similar size, (3) accurate alignment of the knee joint with the hip and the ankle, (4) using feedback controls to predict muscle forces only based on a target length/time curve, and (5) parameter optimization for multibody soft tissue was performed only based on finite element solutions. Future work will include expanding the range and complexity of the activity to capture the entire walk cycle. Obviously, to improve prediction accuracy and reduce uncertainties, developing subject-specific musculoskeletal models from their detailed MRI datasets is suggested. Also, using more sophisticated techniques, such as iterative feedback tuning approaches or applying hill-models to predict muscle forces and muscle activations could improve prediction of joint forces. Finally driving multibody tissue parameters directly from experimental measurements may be help to ensure the validation step.

REFERENCES

"LifeModeler". (2010). Lifemodeler software. Retrieved April 22nd, 2010, from http://www.lifemodeler.com/.

Andriacchi TP, Mundermann A, Smith RL, Alexander EJ, Dyrby CO, and Koo S (2004). "A framework for the in vivo pathomechanics of osteoarthritis at the knee." Ann Biomed Eng. **32**(3):447–457.

Arnold EM, Ward SR, Lieber RL, and Delp SL (2009). "A model of the lower limb for analysis of human movement." Annals of Biomedical Engineering DO1:10.1007/s10439-009-9852-5.

Beaufils P, and Verdonk R (2010). The meniscus. New York: Springer.

Bei Y, and Fregly BJ (2004). "Multibody dynamic simulation of knee contact mechanics." Med Eng Phys **26**(9):777–89.

Blankevoort L, Kuiper JH, Huiskes R, and Grootenboer HJ (1991). "Articular contact in a three-dimensional model of the knee." J Biomech **24**(11):1019–31.

Bullough PG, Munuera L, Murphy J, and Weinstein AM (1970). "The strength of the menisci of the knee as it relates to their fine structure." J Bone Joint Surg Br **52**:564–567.

Erdemir A, Mclean S, Herzog W, and Van Den Bogert AJ (2007) Model-based estimation of muscle forces exerted during movements. Clin Biomech **22**(2):131–54.

Caruntu DI, and Hefzy MS (2004). "3-D anatomically based dynamic modeling of the human knee to include tibio-femoral and patello-femoral joints." J Biomech Eng **126**(1):44–53.

Donahue TL, Hull ML, Rashid MM, and Jacobs CR (2002). "A finite element model of the human knee joint for the study of tibio-femoral contact." J Biomech Eng **124**(3):273–80.

Dye SF (2003). "Functional morphologic features of the human knee: an volutionary perspective." Clin Orthop **410**:19–24.

Englund M, Guermazi A, and Lohmander LS (2009). "The role of the meniscus in knee Osteoarthritis: a Cause or Consequence?" Radiol Clin N Am **47**:703-712.

Englund M, and Lohmander LS (2004). "Risk factors for symptomatic knee osteoarthritis fifteen to twenty-two years after meniscectomy." Arthritis Rheum **50**(9):2811–9.

Englund M, Roos EM, and Lohmander LS (2003). "Impact of type of meniscal tear on radiographic and symptomatic knee osteoarthritis: a sixteen-year followup of meniscectomy with matched controls." Arthritis Rheum **48**(8):2178–87.

Erdemir, A., Mclean, S., Herzog, W., and Van Den Bogert, A. J (2007). "Model-Based Estimation of Muscle Forces Exerted During Movements," Clin Biomech (Bristol, Avon), **22**(2):131-54.

Fithian DC, Kelly MA, and Mow VC (1990). "Material properties and structure-function relationships in the menisci." Clin Orthop Relat Res **252**:19–31.

Fregly, B.J., Besier, T.F., Lloyd, D.G., Delp, S.L., Banks, S.A., Pandy, M.G., and D'Lima, D.D. (2011) "Grand challenge competition to predict in vivo knee loads." Journal of Orthopaedic Research (conditionally accepted).

Fukubayashi T, and Kurosawa H (1980). "The contact area and pressure distribution pattern of the knee. A study of normal and osteoarthrotic knee joints." Acta Orthop Scand **51**:871–879.

Fukubayashi T, Torzilli PA, Sherman MF, and Warren RF. (1982). "An in vitro biomechanical evaluation of anterior-posterior motion of the knee." Tibial displacement, rotation, and torque. J Bone Joint Surg Am **64**:258–264.

Goertzen DJ, Budney DR, and Cinats JG (1997). "Methodology and apparatus to determine material properties of the knee joint meniscus." Med Eng Phys **19**:412–419.

Guess TM, and Maletsky LP (2005). "Computational modeling of a dynamic knee simulator for reproduction of knee loading. J Biomech Eng **127**(7):1216–21.

Guilak F, Butler DL, and Goldstein SA (2001). "Functional tissue engineering: the role of biomechanics in articular cartilage repair." Clin Orthop Relat Res **391**(Suppl.):S295–305.

ISO 14243-1:2002. Implants for surgery –Wear of total knee-joint prostheses – Part 1: Loading and displacement parameters for wear-testing machines with load control and corresponding environmental conditions for test.

Joshi MD, Suh JK, Marui T, and Woo SL (1995). "Interspecies variation of compressive biomechanical properties of the meniscus." J Biomed Mater Res **29**:823–828.

Kim, H. J., Fernandez, J. W., Akbarshahi M, Walter JP, Fregly BJ, and Pandy MG (2009). "Evaluation of predicted knee-joint muscle forces during gait using an instrumented knee implant." Journal of Orthopaedic Research, **27**(10), 1326-1331.

Kurosawa H, Fukubayashi T, and Nakajima H (1980). "Loadbearing mode of the knee joint: physical behavior of the knee joint with or without menisci." Clin Orthop Relat Res **149**:283–290.

Krause WR, Pope MH, Johnson RJ, and Wilder DG (1976). "Mechanical changes in the knee after meniscectomy." J Bone Joint Surg Am **58**:599–604.

Lechner K, Hull ML, and Howell SM (2000). "Is the circumferential tensile modulus within a human medial meniscus affected by the test sample location and cross-sectional area?" J Orthop Res **18**:945–951.

Levy IM, Torzilli PA, and Warren RF (1982). "The effect of medial meniscectomy on anterior-posterior motion of the knee." J Bone Joint Surg Am Vol **64**:883–888.

Levy IM, Torzilli PA, Gould JD, and Warren RF (1989). "The effect of lateral meniscectomy on motion of the knee." J Bone Joint Surg Am **71**:401–406.

Li G, Lopez O, and Rubash H (2001). "Variability of a three dimensional finite element model constructed using magnetic resonance images of a knee for joint contact stress analysis." J Biomed Eng. **123**:341–346.

Li, G., Gil J, Kanamori A, and Woo SL (1999). "A validated three-dimensional computational model of a human knee joint." Journal of Biomech Eng 121, no. 6: 657-62.

Li G, Suggs J, and Gill T (2002). "The effect of anterior cruciate ligament injury on knee joint function under a simulated muscle load: a three-dimensional computational simulation." Ann Biomed Eng. **30**:713–720.

Maletsky LP, and Hillberry BM. (2005). "Simulating dynamic activities using a five-axis knee simulator." J Biomech Eng **127**(1):123–33.

Maletsky LP, Sun J, and Morton NA (2007). "Accuracy of an optical active-marker system to track the relative motion of rigid bodies." J Biomech **40**(3):682–5.

Markolf KL, Bargar WL, Shoemaker SC, and Amstutz HC (1981). "The role of joint load in knee stability." J Bone Joint Surg Am **63**:570–585.

Messner K, and Gao J (1998). "The menisci of the knee joint. Anatomical and functional characteristics, and a rationale for clinical treatment." J Anat **193**(pt 2):161–178.

Mishra M (2010). Computational modeling of tibio-femoral joint. Master thesis.

Morrison JB. (1970). "The mechanics of the knee joint in relation to normal walking." J Biomech **3**:51-61.

Nelson EW, and LaPrade RF (2000). "The anterior intermeniscal ligament of the knee: an anatomic study." Am J Sports Med **28**:74–76.

Nigg M.B and Herzog W (2007). Biomechanics of the Musculo-skeletal System. 3rd edition. USA: John Willy & Sons Ltd.

Orlee KS, and Vaughan CL (1995). " Fundamental patterns of bilateral muscle activity in human locomotion." Biol. Cybern **73**: 409-414

Paiva G (2010). Development of multibody soft tissue models and their tuning to experimental data: With a focus on the canine meniscus. Master thesis.

Pandy MG, Sasaki K, and Kim S. (1998). "A three-dimensional musculoskeletal model of the human knee joint." Comput Methods Biomech Biomed Eng **1**(2):87–108.

Pena E, Calvo B, Martı´nez MA, and Doblare´ M (2006b). "A threedimensional finite element analysis of the combined behavior of ligaments and menisci in the healthy human knee joint." J Biomech. **39**:1686–1701.

Pena E, Calvo B, Martı´nez MA, and Doblare´ M (2008). "Computer simulation of damage on distal femoral articular cartilage after meniscectomies." Comput Biol Med. **38**:69–81.

Pena E, Calvo B, Martı´nez MA, Palanca D, and Doblare´ M (2005). "Finite element analysis of the effect of meniscal tears and meniscectomies on human knee biomechanics." Clin Biomech. **20**:498–507.

Pena E, Calvo B, Martı´nez MA, Palanca D, and Doblare´ M (2006a). "Why lateral meniscectomy is more dangerous than medial meniscectomy. A finite element study." J Orthop Res. **24**(5):1001–1010.

Penrose JM, HoltGM,Beaugonin M, and Hose DR (2002). "Development of an accurate three dimensional finite element knee model." Comput Methods Biomech Biomed Eng **5**(4):291–300.

Piazza SJ, and Delp SL (2001). "Three-dimensional dynamic simulation of total knee replacement motion during a step-up task." J Biomech Eng **123**(6):599–606.

Proctor CS, Schmidt MB, Whipple RR, Kelly MA, and Mow VC (1989). "Material properties of the normal medial bovine meniscus." J Orthop Res **7**:771–782.

Renstrom P, and Johnson RJ (1990). "Anatomy and biomechanics of the menisci." Clin Sports Med **9**:523–538.

Sasaki K, and Neptune RR (2010). "Individual muscle contributions to the axial knee joint contact force during normal walking." Journal of Biomech **43**:2780-2784.

Seedhom BB (1976) Loadbearing function of the menisci. Physiotherapy **62**:223.

Sharf I, and Zhang Y (2006). "A contact force solution for non-colliding contact dynamics simulation." Multibody Syst Dyn **16**(3):263–90.

Sohn DH, and Toth AP (2008). "Meniscus transplantation: current concepts." J Knee Surg **21**(2):163–72.

Sommerlath K, and Gillquist J (1992). "The effect of a meniscal prosthesis on knee biomechanics and cartilage. An experimental study in rabbits." Am J Sports Med **20**:73–81.

Strickland AM (2009). Enhanced pre-clinical assessment of total knee replacement using computational modeling with experimental corroboration and probabilistic application. Doctoral dissertation.

Stylianou A, Guess TM, Olcott L, Paiva G, Kia M, and Cook J (2011). "Validation of a subject specific canine stifle joint model" Proceedings of the ASME 2011 Summer Bioengineering Conference

Sweigart MA, Zhu CF, Burt DM, DeHoll PD, Agrawal CM, Clanton TO, and Athanasiou KA (2004). "Intraspecies and interspecies comparison of the compressive properties of the medial meniscus." Ann Biomed Eng **32**:1569–1579

Tissakht M, and Ahmed AM (1995). "Tensile stress-strain characteristics of the human meniscal material." J Biomech **28**:411–422

Van Tienen TG, Hannink G, and Buma P (2009). "Meniscus replacement using synthetic materials." Clin Sports Med **28**(1):143–56.

Vaughan CL, Davis BL, and O'Connor CJ (1999). Dynamics of human gait. South Africa: Kiboho.

Vedi V, Williams A, Tennant SJ, Spouse E, Hunt DM, and Gedroyc WM (1999). "Meniscal movement. An *in-vivo* study using dynamic MRI." J Bone Joint Surg **81**:37–41

Winter DA (2009). Biomechanics and motor control of human movement. 4th edition. USA: John Willy & Sons Ltd.

Wismans J, Veldpaus F, Janssen J, Huson A, and Struben P. (1980). "A three-dimensional mathematical model of the knee-joint." J Biomech **13**(8):677–85.

Yang NH, Canvan PK, Nayeb Hashemi H, Najafi B, and Vaziri A (2010). "Protocol for constructing subject-specific biomechanical models of knee joint." Comp Meth Biomech and Biomed Eng **13**: 589–603.

Yao J, Lancianese SL, Hovinga KR, LeeJ, and Lerner AL (2008). "Magnetic resonance image analysis of meniscal translation and tibio-menisco-femoral contact in deep knee flexion." J Orthop Res **26**(5):673–684.

Zatsiorsky, VM (1998). Kinematics of Human Motion, Human Kinetics, Champaign, IL.

Zhao D, Banks SA, D'lima DD, Colwell Jr CW, and Fregly BJ (2007). "In vivo medial andlateral tibial loads during dynamic and high flexion activities." J Orthop Res **25**(5):593–602.

Zielinska B, and Donahue TL (2006). "3D finite element model of meniscectomy: changes in joint contact behavior." J Biomech Eng **128**(1):115–23.

VITA

Mohammad Kia was born on June 20, 1980, in Noshahar, Iran. He attended local public schools and graduated with "outstanding honors" from Emam Ali High School in 1998. The same year, he enrolled at the Iran University of Science and Technology (IUST) and began studying mechanical engineering, his area of interest. In the fall of 2002, he graduated with a Bachelor of Science degree in Mechanical Engineering.

He entered in the Khaje Nasir Toosi University of Technology (KNTU) in Iran, in the fall of 2003, and began working as a graduate research assistant and a software engineering support specialist. In addition, he had a chance to work closely with a car company's engineers and design teams on issues related to his final thesis project. In the spring of 2006, he graduated with a Master of Science degree in Mechanical Engineering, with an emphasis in vehicle dynamics.

After moving to the United States in July 2006, Mohammad started pursuing his Ph.D. in Mechanical Engineering, with an emphasis in Biomechanics, at the University of Missouri-Kansas City (UMKC). In January 2007, he joined the Musculoskeletal Biomechanics Research Laboratory as a graduate research assistant. He spent five full years working in the biomechanical lab under the direction of Dr. Trent Guess. Throughout his academic years, he gained considerable experience at developing a multi-scale model of human knee joints. He also served as a teaching assistant for the Instruments and Measurements Lab I and II courses in his fourth year of doctoral study. Upon completion of his degree requirements for a doctoral degree in Mechanical Engineering, Mohammad plans to use his education to follow a career in vehicle safety and injury biomechanics.